Determination of orientation of the ground state using two-photon nonresonant excitation

Andrew C. Kummel, Greg O. Sitz, and Richard N. Zare
Department of Chemistry, Stanford University, Stanford, California 94305-5080

(Received 19 October 1987; accepted 18 December 1987)

A method is presented for determining the population $A_{0+}^{\{0\}}$, the alignment factors $A_{q\pm}^{\{2\}}$ and $A_{q\pm}^{\{4\}}$, and the orientation factors $A_{q\pm}^{\{1\}}$ and $A_{q\pm}^{\{3\}}$ for a ground state distribution of diatomic (symmetric top) molecules probed by elliptically polarized two-photon nonresonant excitation. General expressions are developed for the *O*, *P*, *Q*, *R*, and *S* branch transitions as a function of the rotational quantum number, *J*. This treatment assumes that the resonant state reached by the two-photon transition is subsequently detected independent of its orientation and alignment. This can be achieved by $2+n$ multiphoton ionization in which the ionization steps are saturated, or by $2+1$ laser induced fluorescence in which the fluorescence is collected independent of its polarization and spatial anisotropy. For the case where elliptically polarized light is created by passing linearly polarized light through a quarter-wave plate, the alignment and orientation moments can be independently determined using a single experimental excitation–detection geometry.

I. INTRODUCTION

This paper presents the theory required to determine the orientation of an ensemble of molecules using two-photon nonresonant excitation. By orientation we mean the net helicity of the angular momentum vector, **J**. In the $|JM\rangle$ representation, orientation implies that there are unequal probabilities that the molecule is in sublevel M as opposed to sublevel $-M$. This paper treats the most general case: detection of population, alignment, and orientation by elliptically polarized light which has been prepared using a variable phase shift wave plate propagating along any spatial direction. By varying the ellipticity one can determine, in principle, the 25 $A_{q\pm}^{\{k\}}$ for $k \leqslant 4$. Elliptically polarized light is of great experimental utility because it permits the determination of several orientation moments using a single experimental geometry. In contrast, with circularly and linearly polarized light one must employ several experimental geometries in order to extract multiple orientation moments. There are three important geometries for using elliptically polarized light in conjunction with two-photon nonresonant excitation: light which has been prepared with half- and quarter-wave plates which is propagating along either the *x*, *y*, or *z* laboratory axes. We will present the specific formulas for these three cases as well as a completely general formula. This paper is a direct extension of our previous work[1] (hereafter denoted as KSZ) for determining the population and alignment of the ground state by two-photon nonresonant excitation with linearly polarized light.

Much work has addressed the extraction of the population and alignment of the ground state distribution using linearly polarized light in conjunction with laser induced fluorescence (LIF) or multiphoton ionization (MPI) (see Ref. 1 and references cited therein), but very little theoretical work has addressed the problem of determining orientations. Jeyes *et al.*[2] as well as Macek and Burns[3] have derived a theory to extract $A_{0+}^{\{0\}}$, $A_{0+}^{\{1\}}$, and $A_{0+}^{\{2\}}$ from emission spectra. Bain and McCaffery, as well as Bain *et al.*[4] showed how to determine $A_{0+}^{\{0\}}$, $A_{0+}^{\{1\}}$, and $A_{0+}^{\{2\}}$ using single-photon absorption spectroscopy. Bain and McCaffery[5] also demonstrated how $A_{0+}^{\{0\}}$, $A_{0+}^{\{1\}}$, $A_{0+}^{\{2\}}$, $A_{0+}^{\{3\}}$, and $A_{0+}^{\{4\}}$ can be determined using two-photon absorption, $2+n$ MPI, but they only give explicit formulas for $\Delta J = \pm 2$ transitions. In their papers, McCaffery and co-workers restrict themselves to linearly and circularly polarized light and to determining only the $A_{q\pm}^{\{k\}}$ with $q=0$. Case, McClelland, and Herschbach[6] have derived a very general formalism for $1+1$ LIF which allows, in principle, the determination of any of the $A_{q\pm}^{\{k\}}$; however, their paper also considers only linearly and circularly polarized light.

Several experiments have exploited the permanent dipole of CX_3Y or AB to orient the angular momentum of these molecules. These oriented molecules were subsequently reacted with an atom beam,[7–10] scattered off a molecular beam,[11] or photodissociated.[12] The reactivities into all product internal states were studied as a function of the reagent orientation; none of these experiments directly measured molecular orientation by a laser technique.

Atomic orientation has been observed in many beam-foil experiments (see Ref. 3 and references cited therein). In these experiments a high energy ion beam is aimed at a tilted metal foil. The metal atoms recoiling off the foil are both oriented and electronically excited and hence produce elliptically polarized emission.

The experiments most relevant to this paper have been done by McCaffery and co-workers and by ourselves. Jeyes *et al.*[2] used circularly polarized light to prepare single rovibronic states of I_2^* with a known alignment and orientation. They allowed the I_2^* to collide with He and calculated the remaining orientation by measuring the circular polarization ratio from the emission of I_2^*. Jeyes, McCaffery, and Rowe[13] did similar experiments on Li_2. In each case they could measure only one orientation parameter, $A_{0+}^{\{1\}}$, because their probe was a one-photon process.

In general, there may be many orientation parameters

 0021-9606/88/116707-26$02.10

and measuring a circular polarization ratio (for example, the degree of circular polarization) either in absorption or emission does not provide sufficient information to determine multiple orientation moments. This paper presents formulas which allow data taken with elliptically polarized light to be analyzed so that several orientation moments can be determined. Recently, Sitz, Kummel, and Zare[14] have measured two orientation moments for N_2 scattered off Ag(111). They used 2 + 2 multiphoton ionization to detect the N_2 and the results presented in this paper to analyze the data.

This paper is a companion to KSZ, and hence we assume that the reader is already familiar with the equations in that paper.[1] The only equations we will derive are those that differ from the ones in our previous paper. Section II presents the general equations needed to convert raw data taken with elliptically polarized light into moments of the ground state distribution. This section also contains the simple formulas that are applicable for three special cases: light propagating parallel or antiparallel to the x, y, or z axes. These results are summarized in Tables I–IX, and the derivations are given in the Appendix. In Sec. III we calculate the line strength factors and demonstrate how to extract the polarization moments from experiments for the three special cases for a sample molecule. In Sec. IV we discuss the meaning of the higher order orientation moments. In Sec. V we consider the effects of using a variable wave plate or incoherent light upon the two-photon absorption process. In Sec. VI we derive the two-photon absorption probability for specific $|JM\rangle$ states in order to gain insight into the two-photon absorption process using elliptically polarized light.

II. ABSORPTION PROBABILITY FOR ELLIPTICALLY POLARIZED LIGHT

We can readily adapt the generalized equations from KSZ by expressing the expansion of the absorption intensity in terms of the sum over all ranks and components of the moments of the line strength $P^{\{k\}}_{q\pm}$ and the moments of the ground state distributions $A^{\{k\}}_{q\pm}$. In addition, we must include in the equation for $P^{\{k\}}_{q\pm}$ the sum over all ranks of the squares of the first and second photons absorbed, k_d and k_a. Hence the intensity of a two-photon resonant absorption from ground state J_i,Λ_i to the virtual state J_e,Λ_e and then to the resonant final state J_f,Λ_f is as follows:

$$I = C(\det)n(J_i)\sum_{k,q}\left[P^{\{k\}}_{q+}(J_i,\Lambda_i,J_f,\Lambda_f;\Omega)A^{\{k\}}_{q+}(J_i) + P^{\{k\}}_{q-}(J_i,\Lambda_i,J_f,\Lambda_f;\Omega)A^{\{k\}}_{q-}(J_i)\right], \quad (1)$$

where

$$P^{\{k\}}_{q\pm}(J_i,\Lambda_i,J_f,\Lambda_f;\Omega) = b^k(J_i)g^k(J_i)\sum_{k_d,k_a}(-1)^k\epsilon^{\{k\}}_{q\pm}(k_d,k_a;\Omega_{\rm lab}) \times \sum_{J_e,\Lambda_e,J'_e,\Lambda'_e} S(J_i,\Lambda_i,J_e,\Lambda_e,J'_e,\Lambda'_e,J_f,\Lambda_f) \times h(k_d,k_a,k,J_i,J_e,J'_e,J_f), \quad (2)$$

where $k = 0,1,2,3,4$, $q = 0,1,2,3,4$, but $q \leqslant k$ and $k_d = 0,1,2$ and $k_a = 0,1,2$. As with linearly polarized light, J_e,Λ_e, and J'_e,Λ'_e are subject to the usual dipole selection rules with respect to J_i,Λ_i and J_f,Λ_f.

As indicated by the brackets around the ranks of the tensors[1] in Eqs. (1) and (2), we are employing the Hertel–Stoll[15] normalization for the spherical tensor operators. This is of great utility when determining moments of the ground state distribution with nonzero components since all $A^{\{k\}}_{q\pm}$ are real in the Hertel–Stoll normalization but complex in the standard normalization. As explained in the Appendix, this renormalization reduces the number of detectable moments because sometimes we can detect only the real or imaginary part of a complex A^k_q.

In Eqs. (1) and (2) most of the terms have the same definitions as in KSZ: the detection-sensitivity constant $C(\det)$, the population $n(J_i)$, the moments of the ground state distributions $A^{\{k\}}_{q\pm}$, the moments of the line strength $P^{\{k\}}_{q\pm}$, the reduced matrix elements of the spherical tensor angular momentum operators $b^k(J_i)$, the hyperfine and spin depolarization $g^k(J_i)$ and $g^k(N_i)$, the reduced matrix elements of the dipole moment operator $S(J_i,\Lambda_i,J_e,\Lambda_e,J'_e\Lambda'_e,J_f,\Lambda_f)$, and the angular momentum coupling terms $h(k_d,k_a,k,J_i,J_e,J'_e,J_f)$. Since KSZ did not deal with the odd moments of the ground state distribution, we need to evaluate the normalization constants for $k = 1,3$. In addition we need to calculate both $A^{\{k\}}_{q\pm}$ and $b^k(J_i)$ for $k = 1,3$ and all q. The only term whose definition is changed by the light being elliptically polarized is the geometric factor $\epsilon^{\{k\}}_{q\pm}(k_d,k_a;\Omega_{\rm lab})$.

In order to determine the polarization parameters $A^{\{k\}}_{q\pm}$ in Eq. (1), we measure the absorption intensity as a function of the laser polarization. The line strengths $P^{\{k\}}_{q\pm}$ can be calculated, but the detection sensitivity constant $C(\det)$ and the rotational populations $n(J_i)$ must also be measured in order to determine the $A^{\{k\}}_{q\pm}$. Often, it is impossible to measure $C(\det)$ and $n(J_i)$, and hence only the unreduced polarization moments can be determined from Eq. (1). The unreduced moments $a^{\{k\}}_{q\pm}$ are equal to the more familiar $A^{\{k\}}_{q\pm}$ multiplied by $a^{\{0\}}_{0+}$:

$$a^{\{k\}}_{q\pm}(J_i) = A^{\{k\}}_{q\pm}(J_i)n(J_i)C(\det), \quad (3)$$

$$A^{\{k\}}_{q\pm}(J_i) = a^{\{k\}}_{q\pm}(J_i)/a^{\{0\}}_{0+}(J_i), \quad (4)$$

$$a^{\{0\}}_{0+}(J_i) = n(J_i)C(\det), \quad (5)$$

$$A^{\{0\}}_{0+}(J_i) = 1. \quad (6)$$

Tables I and II summarize the relevant equations taken from KSZ along with the general equation for $\epsilon^{\{k\}}_{q\pm}(k_d,k_a;\Omega_{\rm lab})$. Table III contains the equations for $\epsilon^{\{k\}}_{q\pm}(k_d,k_a;\Omega_{\rm lab})$ specific to the three special system geometries. Table IV contains the normalization constants for $A^{\{k\}}_{q\pm}$. Tables V–VIII contain the definitions and magic angles for $A^{\{k\}}_{q\pm}$ for all k and q. Table IX lists the values of $b^k(J_i)$ for all k.

A. The general system geometry

For calculating the general equation for $\epsilon^{\{k\}}_{q\pm}(k_d,k_a;\Omega_{\rm lab})$, we employ the standard geometry proposed by Fano[16] (see Fig. 1). In the detector frame of the

TABLE I. The two-photon transition probability for noncoincident lab and detector frames where the detection geometry is general.

$$I = C(\det)n(J_i)\sum_{k,q}\left[P^{\{k\}}_{q+}(J_i,\Lambda_i,J_f,\Lambda_f;\Omega)A^{\{k\}}_{q+}(J_i) + P^{\{k\}}_{q-}(J_i,\Lambda_i,J_f,\Lambda_f;\Omega)A^{\{k\}}_{q-}(J_i)\right]$$

$$P^{\{k\}}_{q+}(J_i,\Lambda_i,J_f,\Lambda_f;\Omega) = b^k(J_i)g^k(J_i)\sum_{k_d,k_a}\left[(-1)^{(k)}\epsilon^{\{k\}}_{q+}(k_d,k_a;\Omega_{\rm lab})\right.$$

$$\left.\times\sum_{J_e\Lambda_e J'_e\Lambda'_e} S(J_i,\Lambda_i,J_e,\Lambda_e,J'_e,\Lambda'_e,J_f,\Lambda_f)h(k_d,k_a,k,J_i,J_e,J'_e,J_f)\right] \text{ where } k=0,1,2,3,4;\ q=0,1,2,3,4 \text{ but } q\leqslant k;\ k_d=0,1,2;\ k_a=0,1,2$$

$$A^{\{k\}}_{q\pm}(J_i) = c(k)\langle(J_iM_i\Lambda_i|J^{\{k\}}_{q\pm}|J_iM_i\Lambda_i)\rangle/[(J_iM_i\Lambda_i|\mathbf{J}^2|J_iM_i\Lambda_i)]^{k/2}$$

$$\epsilon^{\{k\}}_{q+}(k_d,k_a;\Omega_{\rm lab}) = (-1)^q(2-\delta_{q,0})^{1/2}\mathrm{Re}[\epsilon^{(k)}_q(k_d,k_a;\Omega_{\rm lab})],\quad q\geqslant 0$$

$$\epsilon^{\{k\}}_{q-}(k_d,k_a;\Omega_{\rm lab}) = (-1)^q(2)^{1/2}(1-\delta_{q,0})\mathrm{Im}[\epsilon^{(k)}_q(k_d,k_a;\Omega_{\rm lab})],\quad q\geqslant 0$$

$$\epsilon^{(k)}_q(k_d,k_a;\Omega_{\rm lab}) = \sum_{q'} e^{iq'\chi}d^k_{q',q}(-\theta)e^{iq\phi}\sum_m (-1)^{k_a-k_d-q'}(2k+1)^{1/2}\begin{pmatrix}k_d & k_a & k\\ m & q'-m & -q'\end{pmatrix}E^{k_d}_m E^{k_a}_{q'-m}$$

$$E^k_q = [e^{*(1)}\otimes e^{(1)}]^k_q; \qquad \text{see Table III}$$

$$n(J_i) = \text{population of level } J_i$$

$$b^k(J_i) = c(k)^{-1}\{[(J_iM_i\Lambda_i|\mathbf{J}^2|J_iM_i\Lambda_i)]^{k/2}\}/(J_i||J^{(k)}||J_i)$$

$$g^k(J_i) = \sum_I\sum_{F_i}(2F_i+1)^2\begin{Bmatrix}F_i & F_i & k\\ J_i & J_i & I\end{Bmatrix}^2$$

$$g^k(N_i) = \sum_{J_i}(2J_i+1)^2\begin{Bmatrix}J_i & J_i & k\\ N_i & N_i & S\end{Bmatrix}^2 g^k(J_i)$$

$$S(J_i,\Lambda_i,J_e,\Lambda_e,J'_e,\Lambda'_e,J_f,\Lambda_f) = (J'_e\Lambda'_e||r^{(1)}||J_i\Lambda_i)^*(J_e\Lambda_e||r^{(1)}||J_i\Lambda_i)$$
$$\times(J_f\Lambda_f||r^{(1)}||J'_e\Lambda'_e)^*(J_f\Lambda_f||r^{(1)}||J_e\Lambda_e)$$

$$(J_2\Lambda_2||r^{(1)}||J_1\Lambda_1) = (4\pi/3)^{1/2}R^{(\Lambda_2-\Lambda_1)}_{21}(2J_2+1)^{1/2}(2J_1+1)^{1/2}$$
$$\times(-1)^{(J_2-\Lambda_2)}\begin{pmatrix}J_1 & J_2 & 1\\ \Lambda_1 & -\Lambda_2 & \Lambda_2-\Lambda_1\end{pmatrix}$$

$$(J_2\Lambda_2||r^{(1)}||J_1\Lambda_1)^* = (-1)^{(J_2-J_1)}(J_1\Lambda_1||r^{(1)}||J_2\Lambda_2)$$

$$h(k_d,k_a,k,J_i,J_e,J'_e,J_f) = (-1)^{(J_f+J'_e-k_d+1)}[(2k_d+1)(2k_a+1)(2k+1)]^{1/2}$$
$$\times\begin{bmatrix}J'_e & J_e & k_d\\ 1 & 1 & J_f\end{bmatrix}\begin{bmatrix}J'_e & 1 & J_i\\ J_e & 1 & J_i\\ k_d & k_a & k\end{bmatrix}$$

standard geometry (x_d,y_d,z_d), the light is propagating along the $-z_d$ axis and is initially linearly polarized along a vector $\hat{\mathbf{B}}$. The ellipticity is created using a wave plate, or equivalent device, whose major axis is parallel to x_d. Here, β is defined as the angle between $\hat{\mathbf{B}}$ and x_d, and β is positive in the counterclockwise direction. Hence, as the light passes through the phase shift device, its y_d component experiences a shift δ, relative to its x_d component. The Euler angles, (ϕ,θ,χ), rotate the laboratory frame (x,y,z) into the detector frame where the x_d axis is the major axis of the wave plate, the y_d axis is the minor axis of the wave plate, and the $-z_d$ axis is pointing along the laser beam propagation direction. For this geometry,

$$\epsilon^{\{k\}}_{q+}(k_d,k_a;\Omega_{\rm lab}) = (-1)^q(2-\delta_{q,0})^{1/2}\times\mathrm{Re}[\epsilon^{(k)}_q(k_d,k_a;\Omega_{\rm lab})],\quad q\geqslant 0, \tag{7}$$

$$\epsilon^{\{k\}}_{q-}(k_d,k_a;\Omega_{\rm lab}) = (-1)^q(2)^{1/2}(1-\delta_{q,0})\times\mathrm{Im}[\epsilon^{(k)}_q(k_d,k_a;\Omega_{\rm lab})],\quad q\geqslant 0, \tag{8}$$

where

$$\epsilon^{(k)}_q(k_d,k_a;\Omega_{\rm lab}) = \sum_{q'} e^{iq'\chi}d^k_{q',q}(-\theta)e^{iq\phi}\times\sum_m (-1)^{k_a-k_d-q'}(2k+1)^{1/2}\times\begin{pmatrix}k_d & k_a & k\\ m & q'-m & -q'\end{pmatrix}E^{k_d}_m E^{k_a}_{q'-m} \tag{9}$$

and

$$E^k_q = [e^{*(1)}\otimes e^{(1)}]^k_q. \tag{10}$$

Here, $e^{(1)}$ is the electric field vector of the photons. The electric field vector cross products E^k_q are just trigonometric functions of ξ, the phase shift, and β, the angle between the major axis of the wave plate and the direction of linear polarization of the incident light. For this general geometry, the E^k_q are identical to those for case I as listed in Table III. Equation (9) is very tedious to evaluate: it contains two summations including a summation over reduced matrix elements. In order to simplify Eq. (9) and gain some insight into the geometric factor, we need to restrict our geometry

TABLE II. Nomenclature for the two-photon transition strength formula.

J_i = Rotational quantum number of the "initial"/ground state apart from nuclear spin
J_e = Rotational quantum number of the "excited"/virtual state apart from nuclear spin
J_f = Rotational quantum number of the "final"/resonant state apart from nuclear spin
Λ_i = Orbital angular momentum quantum number of the initial state
Λ_e = Orbital angular momentum quantum number of the excited/virtual state
Λ_f = Orbital angular momentum quantum number of the final state
k_a = The rank for the square of the first photon
k_d = The rank for the square of the second photon
k = The rank for the ground state distribution
q = The component for the ground state distribution
Ω = Angles describing the geometry of the laser beam with respect to the coordinate system for the moments of the ground state distribution
ϕ,θ,χ = Euler angles which rotate the lab into the detector frame
$\hat{\mathbf{B}}$ = The vector along which the laser light is linearly polarized before passing through the quarter-wave plate
β = Angle between the laser polarization vector and the major axis of the quarter-wave plate
Δ = Angle between the major axis of the quarter-wave plate and one of the three lab axes
ξ = The phase shift between the x_d and y_d components of the electric field vector of the light. ξ is determined by a variable phase shift wave plate. For a quarter-wave plate, $\xi = \pi/2$
F_i = Total angular momentum quantum number of the ground state including nuclear spin
I = Nuclear spin quantum number
S = Electronic spin quantum number
N_i = Total angular momentum quantum number apart from spin for Hund's case (b) molecules

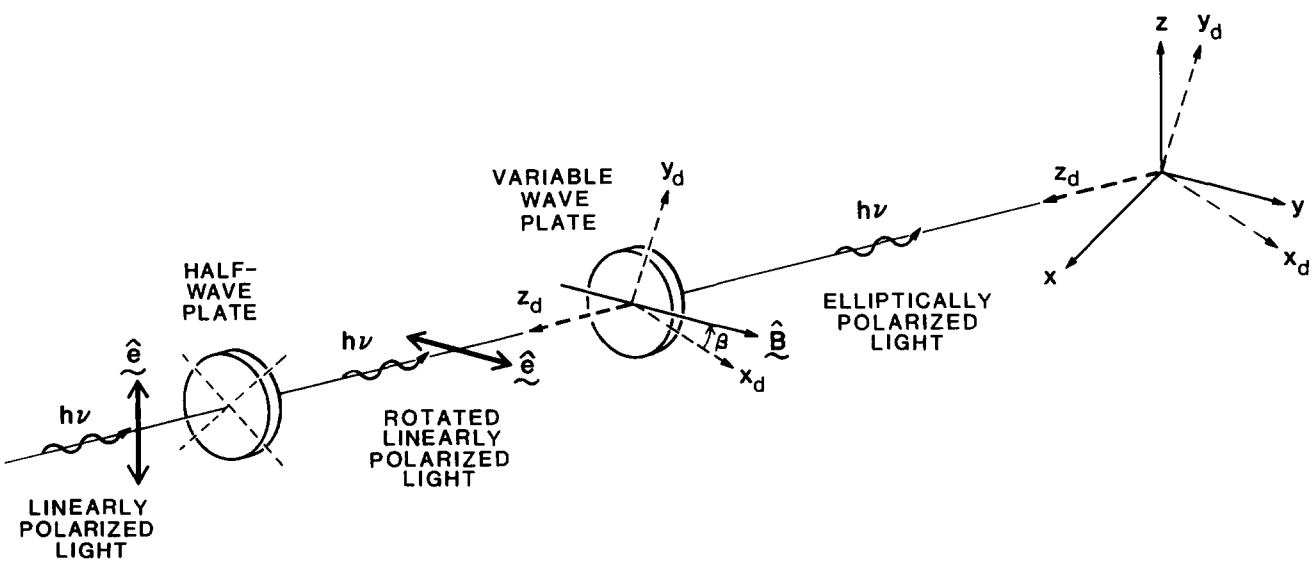

FIG. 1. The standard geometry as defined by Fano (Ref. 16). The linearly polarized light produced by the laser has its electric field vector rotated by a half-wave plate. The variable phase shift wave plate elliptically polarizes the light; the angle between the polarization vector of the rotated linearly polarized light and the major axis of the wave plate determines the ellipticity of the light. The axes of the wave plate and the propagation direction of the light define the detector reference frame relative to the lab reference frame.

by having the laser propagate parallel or antiparallel to the x, y, or z axes.

The laboratory axes are usually assigned so that the z axis is the axis of cylindrical or near-cylindrical symmetry since this minimizes the magnitude of the $A_{q\pm}^{\{k\}}$ with $q \neq 0$. If the molecular ensemble being probed has orientation along only one direction, this direction is labeled as either the x, y, or z axis in order to minimize the number of nonzero $A_{q\pm}^{\{k\}}$ with $k = 1$ or 3.

B. Case I: Propagation along the $-z$ axis

This geometry is similar to the coaxially probed geometry described by Greene and Zare[17] (GZ). The light is propagating along the laboratory $-z$ axis, but the major axis of the wave plate x_d may lie anywhere in the laboratory x–y plane. For case I geometry, β is the angle between $\hat{\mathbf{B}}$ and x_d and Δ is defined as the angle between the x axis and the x_d axis [see Fig. 2(a)]. Since we are free to choose β and Δ, we are free to change the ellipticity and the direction in the x–y plane of the major axis of the ellipsoid of polarization. Then for case I geometry two of the Euler angles are fixed ($\chi = \theta = 0$) and the third is equivalent to $-\Delta$. Consequently, for case I geometry,

$$\epsilon_q^{(k)}(k_d,k_a;\Omega_{\text{lab}}) = [\cos(q\Delta) - i\sin(q\Delta)](-1)^{k_a - k_d - q}(2k+1)^{1/2} \times \sum_m \begin{pmatrix} k_d & k_a & k \\ m & q-m & -q \end{pmatrix} E_m^{k_d} E_{q-m}^{k_a}. \quad (11)$$

This equation is much more convenient than the general equation, Eq. (9), because it avoids the use of the reduced rotation matrices $d_{q',q}^k$, which are tedious to calculate. The E_q^k used in Eq. (11) are the same as for the general geometry and are given in Table III.

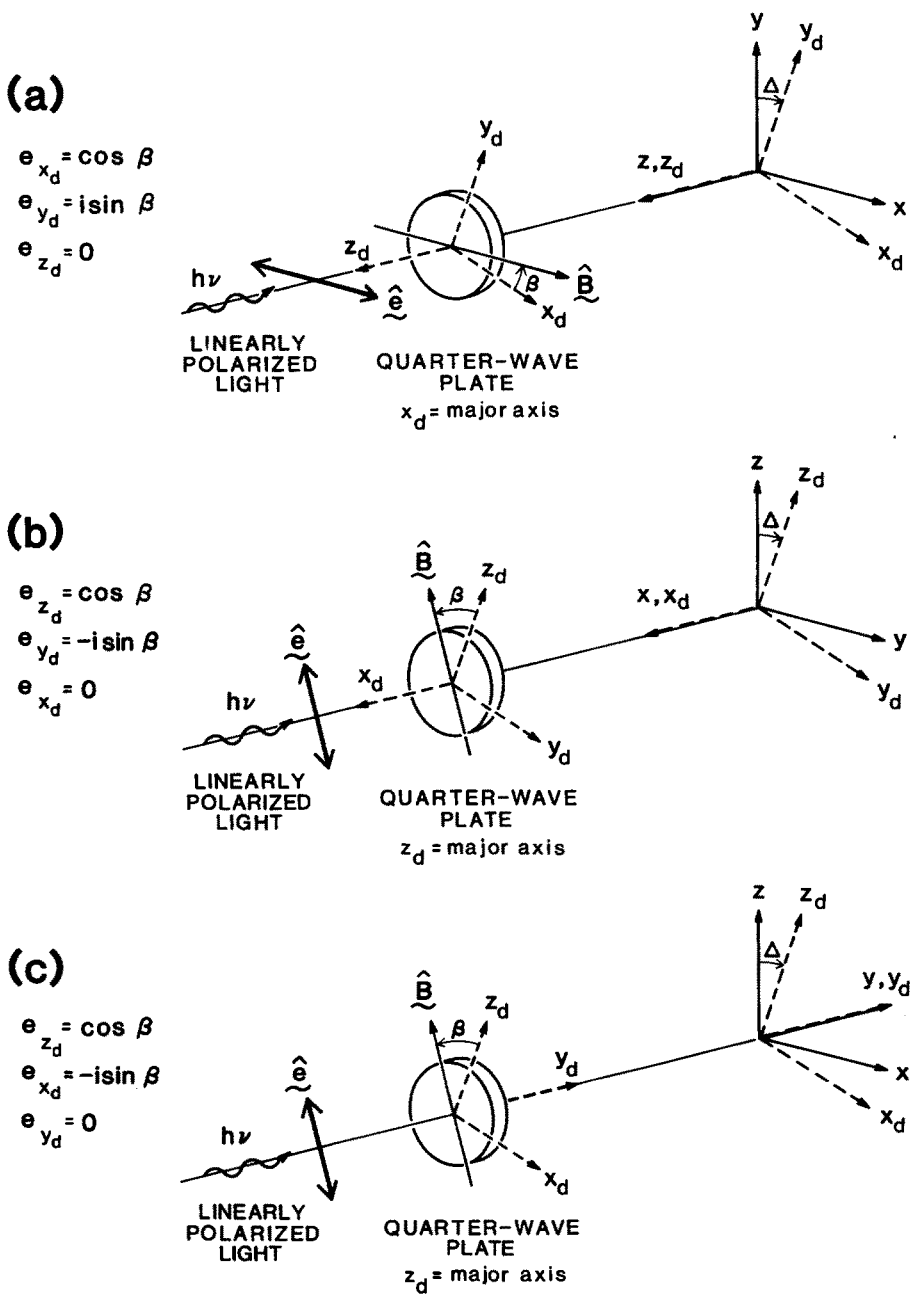

FIG. 2. The reference frames, angles, and electric field vector Cartesian components specific to: (a) case I geometry; (b) case II geometry; and (c) case III geometry.

TABLE III. Simplified equations for the geometry term for cases I, II, and III.

The geometric terms for case I, II, and III geometries

$$\epsilon_q^{(k)}(k_d,k_a;\Omega_{\rm lab}) = [\cos(q\Delta) - i\sin(q\Delta)](-1)^{k_a-k_d-q}(2k+1)^{1/2} \times \sum_m \begin{pmatrix} k_d & k_a & k \\ m & q-m & -q \end{pmatrix} E^{k_d}_m E^{k_a}_{q-m} \quad \text{(case I)}$$

$$\epsilon_q^{(k)}(k_d,k_a;\Omega_{\rm lab}) = [\cos(q\pi/2) + i\sin(q\pi/2)] \sum_{q'} d^k_{q',q}(-\Delta)[\cos(q'\pi/2) - i\sin(q'\pi/2)] \times \sum_m (-1)^{k_a-k_d-q'}(2k+1)^{1/2} \begin{pmatrix} k_d & k_a & k \\ m & q'-m & -q' \end{pmatrix} E^{k_d}_m E^{k_a}_{q'-m} \quad \text{(case II)}$$

$$\epsilon_q^{(k)}(k_d,k_a;\Omega_{\rm lab}) = \sum_{q'} d^k_{q',q}(-\Delta) \sum_m (-1)^{k_a-k_d-q'}(2k+1)^{1/2} \begin{pmatrix} k_d & k_a & k \\ m & q'-m & -q' \end{pmatrix} E^{k_d}_m E^{k_a}_{q'-m} \quad \text{(case III)}$$

The electric field vector cross products E^k_q for light prepared with a quarter-wave plate

E^k_q	Case I	Case II	Case III
E^0_0	$-1/\sqrt{3}$	$-1/\sqrt{3}$	$-1/\sqrt{3}$
$E^1_{\pm 1}$	0	$(\pm 1/2)\sin 2\beta$	$(-i/2)\sin 2\beta$
E^1_0	$(-1/\sqrt{2})\sin 2\beta$	0	0
$E^2_{\pm 2}$	$(1/2)\cos 2\beta$	$(-1/2)\sin^2\beta$	$(1/2)\sin^2\beta$
$E^2_{\pm 1}$	0	0	0
E^2_0	$(-1/\sqrt{6})$	$(1/\sqrt{6})(3\cos^2\beta - 1)$	$(1/\sqrt{6})(3\cos^2\beta - 1)$

The electric field vector cross products E^k_q for light/prepared with a variable wave plate[a]

E^k_q	Case I	Case II	Case III
E^0_0	$-1/\sqrt{3}$	$-1/\sqrt{3}$	$-1/\sqrt{3}$
$E^1_{\pm 1}$	0	$(\pm 1/2)\sin 2\beta \sin\xi$	$(-i/2)\sin 2\beta \sin\xi$
E^1_0	$(-1/\sqrt{2})\sin 2\beta \sin\xi$	0	0
$E^2_{\pm 2}$	$(\cos 2\beta \pm i\sin 2\beta\cos\xi)/2$	$(-1/2)\sin^2\beta$	$(1/2)\sin^2\beta$
$E^2_{\pm 1}$	0	$(i/2)\sin 2\beta\cos\xi$	$(\pm 1/2)\sin 2\beta\cos\xi$
E^2_0	$(-1/\sqrt{6})$	$(1/\sqrt{6})(3\cos^2\beta - 1)$	$(1/\sqrt{6})(3\cos^2\beta - 1)$

[a] Note, we can define ξ' as the deviation of the phase shift from that produced by a quarter-wave plate ($\xi' = 90° - \xi$) and replace $\sin\xi$ with $\cos\xi'$ and $\cos\xi$ with $\sin\xi'$.

C. Case II: Propagation along the $-x$ axis

This geometry is similar to the mutually orthogonal geometry described by GZ. The light is propagating along the laboratory $-x$ axis, and the major axis of the wave plate may lie anywhere in the laboratory y–z plane. Here we define z_d as being parallel to the major axis of the wave plate. For case II, β is the angle between $\hat{\mathbf{B}}$ and the z_d axis, and Δ is the angle between z and z_d [see Fig. 2(b)]. For case II geometry,

$$\epsilon_q^{(k)}(k_d,k_a;\Omega_{\rm lab}) = [\cos(q\pi/2) + i\sin(q\pi/2)] \sum_{q'} d^k_{q',q}(-\Delta)[\cos(q'\pi/2) - i\sin(q'\pi/2)] \times \sum_m (-1)^{k_a-k_d-q'}(2k+1)^{1/2} \begin{pmatrix} k_d & k_a & k \\ m & q'-m & -q' \end{pmatrix} E^{k_d}_m E^{k_a}_{q'-m}. \quad (12)$$

The E^k_q used in Eq. (12) are different from those for Eqs. (9) and (11), and are specific to case II geometry and are given in Table III. For the case where the major axis of the wave plate lies along z, $\Delta = 0$, the reduced rotation matrix $d^k_{q',q}$ in Eq. (12) equals $\delta_{q',q}$, and Eq. (12) is significantly easier to evaluate than Eq. (9).

D. Case III: Propagation along the y axis

This geometry is identical to that used by KSZ. The light is propagating along the laboratory y axis, and the ma-

TABLE IV. Normalization constants for the $A^{\{k\}}_{q\pm}$.

k	$c(k)$	$v(k)$
0	1	$\sqrt{4\pi}$
1	1	$\sqrt{4\pi/3}$
2	$\sqrt{6}$	$\sqrt{8\pi/15}$
3	$\sqrt{10/2}$	$\sqrt{8\pi/35}$
4	$\sqrt{35/8}$	$4\sqrt{2\pi/315}$

TABLE V. The angular momentum spherical tensor operators expressed in the Hertel–Stoll normalization (Ref. 15). Operators with multiple subscripts represent symmetric sums of all unique permutations. For example: $J_{xy} = J_x J_y + J_y J_x$, but $J_{x^2} = (J_x)^2$. $\langle|\mathbf{J}^2|\rangle$ is the magnitude of the vector squared, i.e., $\langle|\mathbf{J}|\rangle = [J(J+1)]^{1/2}$.[a]

$J^{\{0\}}_{0+} = 1$

$J^{\{1\}}_{1-} = J_y$
$J^{\{1\}}_{0+} = J_z$
$J^{\{1\}}_{1+} = J_x$

$J^{\{2\}}_{2-} = (2)^{-1/2} J_{xy}$
$J^{\{2\}}_{1-} = (2)^{-1/2} J_{yz}$
$J^{\{2\}}_{0+} = (1/6)^{1/2} (3J_{z^2} - \mathbf{J}^2)$
$J^{\{2\}}_{1+} = (2)^{-1/2} J_{xz}$
$J^{\{2\}}_{2+} = (2)^{-1/2} (J_{x^2} - J_{y^2})$

$J^{\{3\}}_{3-} = [(1/2)](J_{yx^2} - J_{y^3})$
$J^{\{3\}}_{2-} = [(6)^{-1/2}] J_{xyz}$
$J^{\{3\}}_{1-} = [(15)^{-1/2}/2](4J_{yz^2} - 3J_{y^3} - J_{x^2y})$
$J^{\{3\}}_{0+} = [(1/10)^{1/2}] J_z (5J_{z^2} - 3\mathbf{J}^2 + 1)$
$J^{\{3\}}_{1+} = [(15)^{-1/2}/2](4J_{xz^2} - 3J_{x^3} - J_{xy^2})$
$J^{\{3\}}_{2+} = [(6)^{-1/2}](J_{x^2z} - J_{y^2z})$
$J^{\{3\}}_{3+} = [(1/2)](J_{x^3} - J_{xy^2})$

$J^{\{4\}}_{4-} = [(2)^{-1/2}/2](J_{x^3y} - J_{y^3x})$
$J^{\{4\}}_{3-} = (1/4)(J_{x^2yz} - J_{y^3z})$
$J^{\{4\}}_{2-} = [(14)^{-1/2}/2](2J_{xyz^2} - J_{x^3y} - J_{xy^3})$
$J^{\{4\}}_{1-} = [(7)^{-1/2}/4](4J_{yz^3} - 3J_{y^3z} - J_{x^2yz})$
$J^{\{4\}}_{0+} = [(70)^{-1/2}/2](3\mathbf{J}^4 - 6\mathbf{J}^2 - 30J_{z^2}\mathbf{J}^2 + 25J_{z^2} + 35J_{z^4})$
$J^{\{4\}}_{1+} = [(7)^{-1/2}/4](4J_{xz^3} - 3J_{x^3z} - J_{xy^2z})$
$J^{\{4\}}_{2+} = [(14)^{-1/2}](J_{x^2z^2} - J_{y^2z^2} + J_{y^4} - J_{x^4})$
$J^{\{4\}}_{3+} = (1/4)(J_{x^3z} - J_{xy^2z})$
$J^{\{4\}}_{4+} = [(2)^{-1/2}/2](J_{x^4} + J_{y^4} - J_{x^2y^2})$

[a] $J^{(2)}_{\pm 1}$ and $(J_\pm)^4$ in Table VI of KSZ were incorrectly listed. The correct values are: $J^{(2)}_{\pm 1} = \mp J_\pm (2J_z \pm 1)/2$ and $(J_\pm)^4 = J_{x^4} + J_{y^4} - J_{y^2x^2} \pm i(J_{yx^3} - J_{xy^3})$. Also $J^{(4)}_{\pm 2}$ and $J^{(4)}_0$ are incorrect in Table I of CMH. The correct values are: $J^{(4)}_{\pm 2} = [(J_{x^2z^2} - J_{y^2z^2} + J_{y^4} - J_{x^4}) \pm (i/2)(2J_{xyz^2} - J_{x^3y} - J_{xy^3})]/2\sqrt{7}$ and $J^{(4)}_0 = [(2J_{z^4} - J_{x^2z^2} - J_{y^2z^2}) + (1/4)(3J_{x^4} + 3J_{y^4} + J_{x^2y^2})][2(70)^{-1/2}]$. To generate the $J^{\{k\}}_{q\pm}$ we employed Table I of CMH (with the aforementioned corrections) except for the tensors with $q = 0$ for which we employed Table VI of KSZ. The CMH formulas were used because they are in a form which can be directly converted into the real-tensor operators while the KSZ formulas were employed for $q = 0$ since they express these spherical tensors as functions of J_z alone.

jor axis of the wave plate may lie anywhere in laboratory the x–z plane. For case III, the z_d is defined as being parallel to the major axis of the wave plate, β is the angle between $\hat{\mathbf{B}}$ and z_d, and Δ is defined as the angle between z and z_d [see Fig. 2(c)]. For case III,

$$\epsilon^{(k)}_q(k_d,k_a;\Omega_{\text{lab}}) = \sum_{q'} d^{k}_{q',q}(-\Delta) \sum_m (-1)^{k_a - k_d - q'} (2k+1)^{1/2} \times \begin{pmatrix} k_d & k_a & k \\ m & q'-m & -q' \end{pmatrix} E^{k_d}_m E^{k_a}_{q'-m}. \tag{13}$$

The E^k_q used in Eq. (13) are specific to case III geometry and are given in Table III. Equation (13) is especially convenient when the major axis of the wave plate lies along z because this makes the reduced rotation matrix $d^k_{q',q}(\Delta = 0)$ in Eq. (13) equal to $\delta_{q',q}$.

TABLE VI. Expressions for the moments of the ground state distribution which can be extracted from a two-photon transition using linearly polarized excitation. The moments employ the GZ normalization and the Hertel–Stoll normalization (Ref. 15). In the classical limit: $A^{\{k\}}_{q\pm} = c(k)v(k)\langle|Y^{\{k\}}_{q\pm}(\theta,\phi)|\rangle$, where $c(k)$ and $v(k)$ are given in Table IV and $Y^{\{k\}}_{q\pm}(\theta,\phi)$ are the spherical harmonics describing the angular momentum vector in the Hertel–Stoll normalization [see Eqs. (54)–(56), (A10), (A11)].[a]

$A^{\{0\}}_{0+} = 1$

$A^{\{1\}}_{1-} = \langle(J_i|J_y/\mathbf{J}|J_i)\rangle$
$A^{\{1\}}_{0+} = \langle(J_i|J_z/\mathbf{J}|J_i)\rangle$
$A^{\{1\}}_{1+} = \langle(J_i|J_x/\mathbf{J}|J_i)\rangle$

$A^{\{2\}}_{2-} = (3)^{1/2}\langle(J_i|(J_{xy})/(\mathbf{J}^2)|J_i)\rangle$
$A^{\{2\}}_{1-} = (3)^{1/2}\langle(J_i|(J_{yz})/(\mathbf{J}^2)|J_i)\rangle$
$A^{\{2\}}_{0+} = \langle(J_i|(3J_{z^2} - \mathbf{J}^2)/(\mathbf{J}^2)|J_i)\rangle$
$A^{\{2\}}_{1+} = (3)^{1/2}\langle(J_i|(J_{xz})/(\mathbf{J}^2)|J_i)\rangle$
$A^{\{2\}}_{2+} = (3)^{1/2}\langle(J_i|(J_{x^2} - J_{y^2})/(\mathbf{J}^2)|J_i)\rangle$

$A^{\{3\}}_{3-} = [(10)^{1/2}/4]\langle(J_i|(J_{yx^2} - J_{y^3})/(\mathbf{J}^3)|J_i)\rangle$
$A^{\{3\}}_{2-} = [(5/3)^{1/2}/2]\langle(J_i|(J_{xyz})/(\mathbf{J}^3)|J_i)\rangle$
$A^{\{3\}}_{1-} = [(2/3)^{1/2}/4]\langle(J_i|(4J_{yz^2} - 3J_{y^3} - J_{x^2y})/(\mathbf{J}^3)|J_i)\rangle$
$A^{\{3\}}_{0+} = (1/2)\langle(J_i|J_z(5J_{z^2} - 3\mathbf{J}^2 + 1)/(\mathbf{J}^3)|J_i)\rangle$
$A^{\{3\}}_{1+} = [(2/3)^{1/2}/4]\langle(J_i|(4J_{xz^2} - 3J_{x^3} - J_{xy^2})/(\mathbf{J}^3)|J_i)\rangle$
$A^{\{3\}}_{2+} = [(5/3)^{1/2}/2]\langle(J_i|J_{x^2z} - J_{y^2z})/(\mathbf{J}^3)|J_i)\rangle$
$A^{\{3\}}_{3+} = [(10)^{1/2}/4]\langle(J_i|(J_{x^3} - J_{xy^2})/(\mathbf{J}^3)|J_i)\rangle$

$A^{\{4\}}_{4-} = [(35)^{1/2}/8]\langle(J_i|(J_{x^3y} - J_{y^3x})/(\mathbf{J}^4)|J_i)\rangle$
$A^{\{4\}}_{3-} = [(70)^{1/2}/16]\langle(J_i|(J_{x^2yz} - J_{y^3z})/(\mathbf{J}^4)|J_i)\rangle$
$A^{\{4\}}_{2-} = [(5)^{1/2}/8]\langle(J_i|(2J_{xyz^2} - J_{x^3y} - J_{xy^3})/(\mathbf{J}^4)|J_i)\rangle$
$A^{\{4\}}_{1-} = [(10)^{1/2}/16]\langle(J_i|(4J_{yz^3} - 3J_{y^3z} - J_{x^2yz})/(\mathbf{J}^4)|J_i)\rangle$
$A^{\{4\}}_{0+} = (1/8)\langle(J_i|(3\mathbf{J}^4 - 6\mathbf{J}^2 - 30J_{z^2}\mathbf{J}^2 + 25J_{z^2} + 35J_{z^4})/(\mathbf{J}^4)|J_i)\rangle$
$A^{\{4\}}_{1+} = [(10)^{1/2}/16]\langle(J_i|(4J_{xz^3} - 3J_{x^3z} - J_{xy^2z})/(\mathbf{J}^4)|J_i)\rangle$
$A^{\{4\}}_{2+} = [(5)^{1/2}/4]\langle(J_i|(J_{x^2z^2} - J_{y^2z^2} + J_{y^4} - J_{x^4})/(\mathbf{J}^4)|J_i)\rangle$
$A^{\{4\}}_{3+} = [(70)^{1/2}/16]\langle(J_i|(J_{x^3z} - J_{xy^2z})/(\mathbf{J}^4)|J_i)\rangle$
$A^{\{4\}}_{4+} = [(35)^{1/2}/8]\langle(J_i|(J_{x^4} + J_{y^4} - J_{x^2y^2})/(\mathbf{J}^4)|J_i)\rangle$

[a] In Table VI of KSZ the $A^{\{k\}}_{q\pm}$ and $A^{(k)}_q$ are correct for $q = 0$ and $q = k$; the other formulas are only correct in the high J limit because the conversion formula to the Hertel–Stoll normalization was incorrectly applied. The list of $A^{\{k\}}_{q\pm}$ given here supersedes the one given in KSZ and the corrections to the list of $A^{(k)}_q$ can be generated as follows: $A^{(k)}_q = (-1)^q (2 - \delta_{q,0})^{-1/2} A^{\{k\}}_{q+}$.

This concludes the presentation of the equations needed to determine the two-photon absorption probability for elliptically polarized light. Now we proceed to illustrate the application of these formulas to a specific system.

III. AN EXAMPLE

In this section we calculate the moments of the line strength for a specific case, the N_2 $a\,^1\Pi_g$–$X\,^1\Sigma_g^+$ transition excited by elliptically polarized light which has been prepared with quarter and half-wave plates. Equations and optimal geometries are described for determining the octupole orientation moments $A^{\{3\}}_{q\pm}$, even when these are much smaller than the dipole orientation moments $A^{\{1\}}_{q\pm}$. We also list all the moments that can be measured using each of our three special geometries. Though it may seem repetitious to give explicit equations for all three geometries, it is important for the experimentalist to know the relative magnitudes

TABLE VII. The sensitivity of case I, II, and III geometries to the $A^{\{k\}}_{q\pm}$.

$A^{\{k\}}_{q\pm}$	Case I	Case II	Case III
$A^{\{0\}}_{0+}$	✓	✓	✓
$A^{\{1\}}_{1-}$			✓
$A^{\{1\}}_{0+}$	✓		
$A^{\{1\}}_{1+}$		✓	
$A^{\{2\}}_{2-}$	0,90		
$A^{\{2\}}_{1-}$		0,90,180	
$A^{\{2\}}_{0+}$	✓	54.7,125.3	54.7,125.3
$A^{\{2\}}_{1+}$			0,90,180
$A^{\{2\}}_{2+}$	45,135	0,180	0,180
$A^{\{3\}}_{3-}$			✓
$A^{\{3\}}_{2-}$	0,90	0,90,180	0.90,180
$A^{\{3\}}_{1-}$			✓
$A^{\{3\}}_{0+}$	✓		
$A^{\{3\}}_{1+}$		✓	
$A^{\{3\}}_{2+}$	45,135		
$A^{\{3\}}_{3+}$		✓	
$A^{\{4\}}_{4-}$	0,45,90,135,180		
$A^{\{4\}}_{3-}$		0,90,180	
$A^{\{4\}}_{2}$	0,90		
$A^{\{4\}}_{1-}$		0,49.1,90,130.9,180	
$A^{\{4\}}_{0+}$	✓	30.6,70.1	30.6,70.1
$A^{\{4\}}_{1+}$			0,49.1,90,130.9,180
$A^{\{4\}}_{2+}$	45,135	0,67.8,112.2,180	0,67.8,112.2,180
$A^{\{4\}}_{3+}$			0,90,180
$A^{\{4\}}_{4+}$	22.5,67.5,112.5,157.5	0,180	0,180

[a] If a geometry is sensitive to a particular moment, it is indicated by either a check or an angle. The angles (in degrees) indicate the magic angles of Δ for the indicated geometry and moment. The underlined magic angles are only valid for linearly polarized light, $\beta = 0$.

of the line strengths in the three geometries. This information will help determine the optimal geometry to employ when measuring a particular set of polarization moments.

Magic angles normally refer to particular sets of Euler angles which force one or more of the moments of the line strength $P^{\{k\}}_{q\pm}$ to vanish. First, in each of our geometries, regardless of the value of Δ, two of the Euler angles are fixed. This alone causes many of the $P^{\{k\}}_{q\pm}$ to vanish. The $A^{\{k\}}_{q\pm}$ corresponding to the nonvanishing $P^{\{k\}}_{\pm}$ are listed in Table VII. Second, for each of our three cases there are several values of Δ which force additional $P^{\{k\}}_{q\pm}$ to vanish; these angles are listed inTable VII. Third, there are at least three values of β which cause some of the $P^{\{k\}}_{q\pm}$ to vanish; when the light is linearly polarized ($\beta = 0$ or $\pm\pi/2$), all the orientation line strengths, $P^{\{k\}}_{q\pm}$ with $k = 1$ or 3, vanish. Hence, if one wishes to determine the alignment in a system possessing both alignment and orientation, one first employs linearly polarized light ($\beta = 0$), and records I vs Δ to determine the alignment. Then, one uses elliptically polarized light to determine the orientation moments.

A. Calculated line strengths for case I geometry

In Fig. 3, we have plotted $P^{\{k\}}_{q\pm}$ vs J_i, the rotational quantum number, for $\beta = \pi/8$ and $\Delta = 22.5°$. We have only plotted the curves for $q = 0$ because the shapes of the curves are identical for all $P^{\{k\}}_{q\pm}$ having the same k. Replotting at a different set of angles (β,Δ) would not change the shapes of any of the curves but would multiply all the values by a constant. Since the shapes are invariant with respect to all the Euler angles, the curves for $P^{\{k\}}_{q\pm}$ vs J_i for case I, case II, and case III geometries are identical, except for a scaling constant.

TABLE VIII. Expressions for the rescaling factors $b^k(J_i)$. These expressions employ the GZ normalization.

$$b^0(J_i) = (2J_i + 1)^{-1/2}$$
$$b^1(J_i) = (2J_i + 1)^{-1/2}$$
$$b^2(J_i) = \{J_i(J_i + 1)/[(2J_i + 3)(2J_i + 1)(2J_i - 1)]\}^{1/2}$$
$$b^3(J_i) = 2J_i(J_i + 1)/[(J_i - 1)(2J_i - 1)(2J_i + 1)(2J_i + 3)(J_i + 2)]^{1/2}$$
$$b^4(J_i) = \frac{4J_i^2(J_i + 1)^2}{[(J_i + 2)(J_i + 1)J_i(J_i - 1)(2J_i + 5)(2J_i + 3)(2J_i + 1)(2J_i - 1)(2J_i - 3)]^{1/2}}$$

TABLE IX. The apparent moments as a function of the reduced moments of the ground state distribution.

Case I geometry

$$A_{0+}^{\{0\}}(\text{app}) = A_{0+}^{\{0\}} - \sqrt{5/4}R(2,0,0,0,J_i,J_f)A_{0+}^{\{2\}} + 9/8R(4,0,,0,0,J_i,J_f)A_{0+}^{\{4\}}$$

$$A_{2+}^{\{2\}}(\text{app}) = A_{2+}^{\{2\}} - \sqrt{3/4}R(4,2,2,2,J_i,J_f)A_{2+}^{\{4\}}$$

$$A_{2-}^{\{2\}}(\text{app}) = A_{2-}^{\{2\}} - \sqrt{3/4}R(4,2-,2,2-,J_i,J_f)A_{2-}^{\{4\}}$$

$$A_{4+}^{\{4\}}(\text{app}) = A_{4+}^{\{4\}}$$

$$A_{4-}^{\{4\}}(\text{app}) = A_{4-}^{\{4\}},$$

where

$$R(k,q\pm,k',q'\pm,J_i,J_f) = \frac{[P_{q\pm}^{\{k\}}(J_i,\Lambda_i,J_f,\Lambda_f,\Delta)/Y_{q\pm}^{\{k\}}(\pi/2,-\Delta)]}{[P_{q'\pm}^{\{k'\}}(J_i,\Lambda_i,J_f,\Lambda_f,\Delta)/Y_{q'\pm}^{\{k'\}}(\pi/2,-\Delta)]}$$

Case II geometry

$$A_{0+}^{\{0\}}(\text{app}) = A_{0+}^{\{0\}} + \sqrt{2}[-\sqrt{5/6}R(2,2,0,0,J_i,J_f)A_{2+}^{\{2\}} + \sqrt{7/10}R(4,4,0,0,J_i,J_f)A_{4+}^{\{4\}} - \sqrt{1/10}R(4,2,0,0,J_i,J_f)A_{2+}^{\{4\}}]$$

$$A_{0+}^{\{2\}}(\text{app}) = A_{0+}^{\{2\}} + \sqrt{2}[\sqrt{1/6}R(2,2,2,0,J_i,J_f)A_{2+}^{\{2\}} - \sqrt{2/7}R(4,4,2,0,J_i,J_f)A_{4+}^{\{4\}} - \sqrt{1/2}R(4,4,2,0,J_i,J_f)A_{2+}^{\{4\}}]$$

$$A_{1-}^{\{2\}}(\text{app}) = A_{1-}^{\{2\}} - \sqrt{6/7}R(4,3-,2,1-,J_i,J_f)A_{3-}^{\{4\}}$$

$$A_{0+}^{\{4\}}(\text{app}) = A_{0+}^{\{4\}} + \sqrt{2}[\sqrt{1/70}R(4,4,4,0,J_i,J_f)A_{4+}^{\{4\}} + \sqrt{2/5}R(4,2,4,0,J_i,J_f)A_{2+}^{\{4\}}]$$

$$A_{1-}^{\{4\}}(\text{app}) = A_{1-}^{\{4\}} + \sqrt{1/7}R(4,3-,4,1-,J_i,J_f)A_{3-}^{\{4\}}$$

where

$$R(k,q\pm,k',q'\pm,J_i,J_f) = \frac{[P_{q\pm}^{\{k\}}(J_i,\Lambda_i,J_f,\Lambda_f,\Delta)/Y_{q\pm}^{\{k\}}(\Delta,\pi/2)]}{[P_{q'\pm}^{\{k'\}}(J_i,\Lambda_i,J_f,\Lambda_f,\Delta)/Y_{q'\pm}^{\{k'\}}(\Delta,\pi/2)]}$$

Case III geometry

$$A_{0+}^{\{0\}}(\text{app}) = A_{0+}^{\{0\}} + \sqrt{2}[\sqrt{5/6}R(2,2,0,0,J_i,J_f)A_{2+}^{\{2\}} + \sqrt{7/10}R(4,4,0,0,J_i,J_f)A_{4+}^{\{4\}} + \sqrt{1/10}R(4,2,0,0,J_i,J_f)A_{2+}^{\{4\}}]$$

$$A_{0+}^{\{2\}}(\text{app}) = A_{0+}^{\{2\}} + \sqrt{2}[-\sqrt{1/6}R(2,2,2,0,J_i,J_f)A_{2+}^{\{2\}} - \sqrt{2/7}R(4,4,2,0,J_i,J_f)A_{4+}^{\{4\}} + \sqrt{1/2}R(4,2,2,0,J_i,J_f)A_{2+}^{\{4\}}]$$

$$A_{1+}^{\{2\}}(\text{app}) = A_{1+}^{\{2\}} + \sqrt{6/7}R(4,3,2,1,J_i,J_f)A_{3+}^{\{4\}}$$

$$A_{0+}^{\{4\}}(\text{app}) = A_{0+}^{\{4\}} + \sqrt{2}[\sqrt{1/70}R(4,4,4,0,J_i,J_f)A_{4+}^{\{4\}} - \sqrt{2/5}R(4,2,4,0,J_i,J_f)A_{2+}^{\{4\}}]$$

$$A_{1+}^{\{4\}}(\text{app}) = A_{1+}^{\{4\}} - \sqrt{1/7}R(4,3,4,1,J_i,J_f)A_{3+}^{\{4\}}$$

where

$$R(k,q\pm,k',q'\pm,J_i,J_f) = \frac{[P_{q\pm}^{\{k\}}(J_i,\Lambda_i,J_f,\Lambda_f,\Delta)/Y_{q\pm}^{\{k\}}(\Delta,0)]}{[P_{q'\pm}^{\{k'\}}(J_i,\Lambda_i,J_f,\Lambda_f,\Delta)/Y_{q'\pm}^{\{k'\}}(\Delta,0)]}$$

[a] Table VIII of KSZ is in error because the equations do not contain the $R(k,q,k',q',J_i,J_f)$ terms.

Because the laser is propagating along the $-z$ axis, the measurement is sensitive only to orientation along the z axis and alignment with respect to the x or y axes. Consequently, case I geometry is insensitive to the expectation values of $(J_x)^n$ or $(J_y)^n$ where n is an odd number, and it follows that this geometry is insensitive to all alignment moments with odd components (see Table VII).

In Fig. 4, we have plotted $P_{q\pm}^{\{k\}}$ vs β, the ellipticity angle, at $\Delta = 22.5°$ for $J_i = 20$; this plot shows how the line strengths vary as the light is changed from right circular polarization to linear polarization to left circular polarization (see Sec. VI for definition of right vs left circularly polarized light). In Fig. 4, for a given k and q only $P_{q+}^{\{k\}}$ or $P_{q-}^{\{k\}}$ is depicted because $P_{q-}^{\{k\}} = c(q)\ P_{q+}^{\{k\}}$ where $c(q) = -\sin(q\Delta)/\cos(q\Delta)$. For even ranks, the values of $P_{q\pm}^{\{k\}}$ are symmetric about $\beta = 0°$, and the values for the O and S branches and for the P and R branches are similar. For the odd ranks, the values of $P_{q\pm}^{\{k\}}$ are asymmetric about $\beta = 0°$ and identically equal to zero at $\beta = 0°$. Also the values are of similar magnitude but of opposite sign for the O and S branches as well as for the P and R branches.

Figure 5 is a plot of $P_{q\pm}^{\{k\}}$ vs Δ for $J_i = 20$ probed by elliptically polarized light, $\beta = 22.5°$. This figure depicts how the line strengths vary as the quarter-wave and the half-wave plates are simultaneously rotated. By changing Δ, we change the angle the major axis of the polarization ellipsoid makes with the x axis; hence, we vary the line strenths of the polarization moments which measure a projection of J onto the plane of polarization of our light, the x–y plane. By the same reasoning, we expect that the sensitivity to the expectation values of $(J_z)^n$ to be independent of Δ. Hence, the line strengths for $q = 0$ are invariant with respect to Δ because

the corresponding $A_{0+}^{\{k\}}$ only depend on the expectation values of $(J_z)^n$; these line strengths are not plotted in Fig. 5, but rather they are given in the figure caption. For $q = 2$ or 4, the $P_{q+}^{\{k\}}$ are symmetric about $\Delta = 90°$ and the $P_{q-}^{\{k\}}$ are asymmetric about $\Delta = 90°$ and identically equal to zero at $\Delta = 90°$. The shapes of the curves depend only on the component of $P_{q+}^{\{k\}}$ or $P_{q-}^{\{k\}}$ and not on the rank; the shapes of the curves of $P_{2+}^{\{2\}}$ and $P_{2+}^{\{4\}}$ are identical as are the shapes for $P_{2-}^{\{2\}}$ and $P_{2-}^{\{4\}}$.

B. Exploiting the magic angles for case I

If we have a system which has no alignment moments greater than quadrupole, (for example a $J = 3/2$ system), we can measure two unreduced moments, $a_{2+}^{\{2\}}$ and $a_{2-}^{\{2\}}$, using linearly polarized light, three magic angles, and just one rotational branch:

$$a_{2+}^{\{2\}} = [I(\Delta = 0°) - R\,]/P_{2+}^{\{2\}}(\Delta = 0°), \tag{14}$$

$$a_{2-}^{\{2\}} = [I(\Delta = 45°) - R\,]/P_{2-}^{\{2\}}(\Delta = 45°), \tag{15}$$

where

$$R = [I(\Delta = 0°) + I(\Delta = 90°)]/2. \tag{16}$$

In order to independently determine the remaining moments $a_{0+}^{\{0\}}$ and $a_{0+}^{\{2\}}$, we need only compare the intensities of two rotational branches at one magic angle, $\Delta = 0°$; preferably the rotational branches will be a pair with very different $P_{0+}^{\{2\}}$, for example O and R but not O and S:

$$I'(J_{f1}) = I(J_{f1}) - P_{2+}^{\{2\}}(J_{f1})a_{2+}^{\{2\}}, \tag{17}$$

$$I'(J_{f2}) = I(J_{f2}) - P_{2+}^{\{2\}}(J_{f2})a_{2+}^{\{2\}}, \tag{18}$$

$$a_{0+}^{\{0\}} = [I'(J_{f1}) - rI'(J_{f2})]/[P_{0+}^{\{0\}}(J_{f1}) - rP_{0+}^{\{0\}}(J_{f2})], \tag{19}$$

$$a_{0+}^{\{2\}} = [I'(J_{f2}) - a_{0+}^{\{0\}}P_{0+}^{\{0\}}(J_{f2})]/P_{0+}^{\{2\}}(J_{f2}), \tag{20}$$

where

$$r = P_{0+}^{\{2\}}(J_{f1})/P_{0+}^{\{2\}}(J_{f2}) \tag{21}$$

and the subscripts "$f1$" and "$f2$" on the J_{fn} are used to differentiate between the different rotational branches. In the above equations $I'(J_{fn})$ are the intensities after the contributions from the $a_{2+}^{\{2\}}$ moment have been removed. In Eqs. (17)–(21) all the line strengths are evaluated for $\beta = 0°$ and $\Delta = 0°$ and for a single J_i.

If we are examining a system with case I geometry which has no orientation moments greater than dipole, then we are only able to detect one orientation, $a_{0+}^{\{1\}}$. To determine this orientation we only need to compare the absorption of left and right circularly polarized light for one rotational branch:

$$a_{0+}^{\{1\}} = [I(\beta = +45°) - I(\beta = -45°)]/[2P_{0+}^{\{1\}}(\beta = +45°)]. \tag{22}$$

If a system possesses both dipole and quadrupole moments but no octupole nor hexadecapole moments, one can still utilize Eqs. (14–22). However, if the system has higher order moments of polarization, a linear least-squares technique must be used.

C. Detection of alignment and orientation for a system with cylindrical symmetry and case I geometry

For a system with cylindrical symmetry about the z axis, only the moments with components equal to zero, $A_{0+}^{\{0\}}$, $A_{0+}^{\{1\}}$, $A_{0+}^{\{2\}}$, $A_{0+}^{\{3\}}$, and $A_{0+}^{\{4\}}$, can be nonzero. For detecting these moments, we must analyze data from an experiment which records I vs β since the moments are insensitive to a change in Δ:

$$\begin{pmatrix} I(J_{f1},\beta_1) \\ I(J_{f2},\beta_2) \\ \cdots \\ \cdots \\ \cdots \\ \cdots \\ \cdots \\ I(J_{fm},\beta_m) \end{pmatrix} = \begin{pmatrix} P_{0+}^{\{0\}}(J_{f1},\beta_1) & P_{0+}^{\{1\}}(J_{f1},\beta_1) & P_{0+}^{\{2\}}(J_{f1},\beta_1) & P_{0+}^{\{3\}}(J_{f1},\beta_1) & P_{0+}^{\{4\}}(J_{f1},\beta_1) \\ P_{0+}^{\{0\}}(J_{f2},\beta_2) & P_{0+}^{\{1\}}(J_{f2},\beta_2) & P_{0+}^{\{2\}}(J_{f2},\beta_2) & P_{0+}^{\{3\}}(J_{f2},\beta_2) & P_{0+}^{\{4\}}(J_{f2},\beta_2) \\ & & \cdots & & \\ & & \cdots & & \\ & & \cdots & & \\ & & \cdots & & \\ & & \cdots & & \\ P_{0+}^{\{0\}}(J_{fm},\beta_m) & P_{0+}^{\{1\}}(J_{fm},\beta_m) & P_{0+}^{\{2\}}(J_{fm},\beta_m) & P_{0+}^{\{3\}}(J_{fm},\beta_m) & P_{0+}^{\{4\}}(J_{fm},\beta_m) \end{pmatrix} \begin{pmatrix} a_{0+}^{\{0\}} \\ a_{0+}^{\{1\}} \\ a_{0+}^{\{2\}} \\ a_{0+}^{\{3\}} \\ a_{0+}^{\{4\}} \end{pmatrix}. \tag{23a}$$

In Eq. (23a) the arguments of the intensity and line strength include a J_{fn} to indicate the rotational branch being probed, and "$n_{\max}$" equals "m." It is important to use at least two rotational branches in order to distinguish between $A_{0+}^{\{1\}}$ and $A_{0+}^{\{3\}}$: the shapes of the plots of $P_{0+}^{\{1\}}$ vs β and $P_{0+}^{\{3\}}$ vs β are very similar for each rotational branch, but the relative magnitudes of these line strengths vary with rotational branch (see Fig. 4). Equation (23a) is very convenient because it allows us to determine the reduced moments of the alignment and orientation directly since Eq. (23a) determines the zeroth moment $a_{0+}^{\{0\}}$.

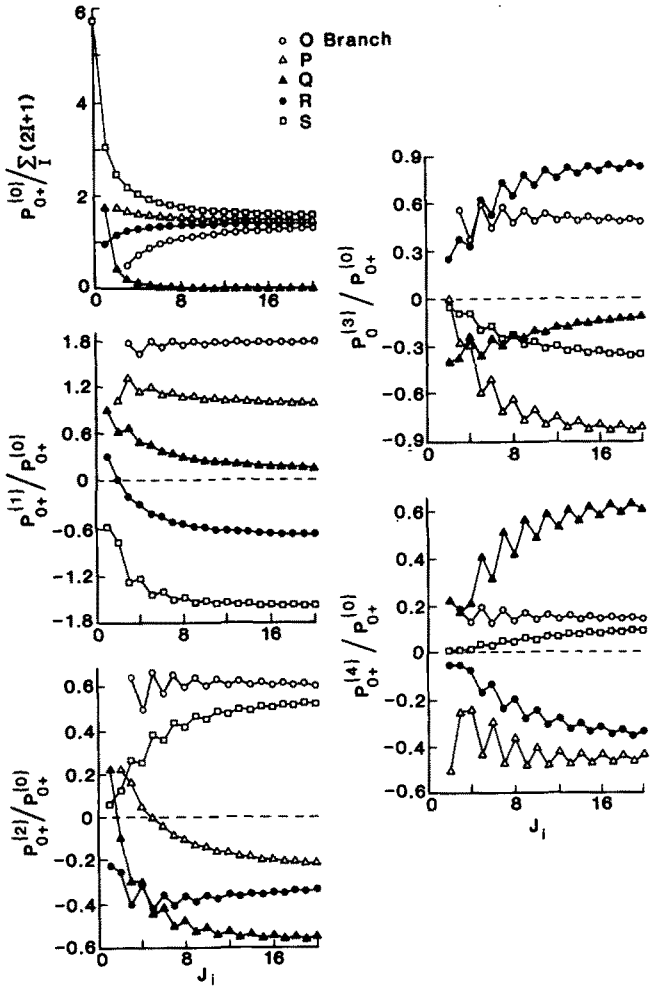

FIG. 3. The moments of the line strength factors $P^{\{k\}}_{0+}$ for case I geometry vs the ground state rotational quantum number for the five rotational branches at $\beta = \pi/8$ and $\Delta = 22.5°$ in the N_2 $a\,^1\Pi_g$–$X\,^1\Sigma_g^+$ two-photon transition. The $P^{\{0\}}_{0+}$ have been normalized with respect to the total nuclear hyperfine degeneracy of each J_i, and the higher order moments have been normalized with respect to the zeroth moment. Note that the labeling of a similar figure in our previous paper, Fig. 5 of KSZ, was misleading; the correct labels are presented here.

Equation (23a) can be written in compact symbolic matrix notation:

$$\vec{I}(J_{fn},\beta_n) = \underset{\sim}{\mathbf{P}}^{\{k\}}_{q\pm}(J_{fn},\beta_n)\vec{a}^{\{k\}}_{q\pm}, \tag{23b}$$

where

$$n = 0 \rightarrow n_{\max}, \tag{23c}$$

$$(k,q) = (0,0+),(1,0+),(2,0+),(3,0+),(4,0+). \tag{23d}$$

Here a vector is indicated by an arrow, and the rectangular array is denoted by a bold letter with a tilde. The horizontal variables in the array are the ranks and components of the moments of the line strength while the vertical variables are the polarization angles and rotational branches. When describing an experiment to determine specific moments, we will employ this matrix notation.

D. Calculated line strengths for case II and III geometries

The shapes of the plots of $P^{\{k\}}_{q\pm}$ vs J_i for cases II and III, for $\beta = 22.5°$ and $\Delta = 22.5°$ are identical to those for case I geometry (see Fig. 3), except for a scaling constant, so they have not been reproduced here. Similar to case I, the shapes of the curves are insensitive to both β and Δ and for a given k all the curves for $P^{\{k\}}_{q\pm}$ vs J_i have the same shape. The other figures of the calculated moments for case II geometry have been combined with those for case III geometry since they are identical except for a phase factor and the signs of the components.

For case II geometry, the laser is propagating along the $-x$ axis; hence, we are only able to detect orientation along the x axis and alignment with respect to either y or z axes. Because of this restriction on detection of orientation, the line strengths for moments with $k = 1,3$ and $q = 0+, 1-, 2+$, or $3-$ are zero. In addition, because of the previously mentioned restriction on alignment detection, the line strengths for moments with $k = 2,4$ and $q = 1+, 2-, 3+$, or $4-$ are also zero.

For case III geometry, the laser light is traveling along the y axis, and, consequently, we are only sensitive to orientation along the y axis and to alignment with respect to the x and z axes. This restriction on orientation sets all the moments of the line strengths to zero for $k = 1$ or 3 with $q \geqslant 0$. The aforementioned restrictions on the alignment set all the line strengths to zero for $k = 2$ or 4 and $q < 0$.

In Fig. 6, we have plotted $P^{\{k\}}_{q\pm}$ vs β, the ellipticity angle, at $\Delta = 22.5°$ for $J_i = 20$ for case II and III geometries. For even ranks, the values of $P^{\{k\}}_{q\pm}$ are symmetric about $\beta = 0°$, and for odd ranks, the values of $P^{\{k\}}_{q\pm}$ are asymmetric about $\beta = 0°$ and identically equal to zero at $\beta = 0°$. For case II and III geometries, there are several magic angles of β: at $\beta = \pm 45°$ $P^{\{2\}}_{1-}$ (cases II and III), $P^{\{3\}}_{2-}$ (cases II and III), $P^{\{4\}}_{1-}$ (case II), $P^{\{4\}}_{1+}$ (case III), $P^{\{4\}}_{3-}$ (case II), and $P^{\{4\}}_{3+}$ (case III) are zero. For both cases II and III if $\beta = 0°$, linearly polarized light, not only are all the orientation moments zero, but if Δ is also zero, all the alignment moments with nonzero components are zero. At $\beta = 90°$, all the orientation moments are zero, and if Δ is also zero, all the alignment moments with odd components are zero.

Figure 7 is a plot of $P^{\{k\}}_{q\pm}$ vs Δ for $J_i = 20$ being probed by elliptically polarized light, $\beta = 22.5°$, with the propagation vector of the light defined by either case II or III geometry. For case II geometry, the light is propagating along the $-x$ axis, and the sensitivity to the expectation values of $(J_x)^n$ is independent of Δ (see Table VII). Consequently, for case II geometry the $P^{\{0\}}_{0+}$ and $P^{\{1\}}_{1+}$ line strengths are independent of Δ; all other moments are functions of the expectation values of $(J_y)^n$ or $(J_z)^n$, and, hence, their line strengths are dependent on Δ [see Eq. (8)]. Similarly, for case III geometry, since the probe light is propagating along the y axis, the sensitivity to the expectation values of $(J_y)^n$ is independent of Δ. Hence, for case III geometry only $P^{\{0\}}_{0+}$ and $P^{\{1\}}_{1-}$ are independent of Δ. All the other $P^{\{k\}}_{q\pm}$ have unique curves because Δ appears in the argument of the reduced rotation matrix in Eq. (9), $d^k_{q',q}(-\Delta)$.

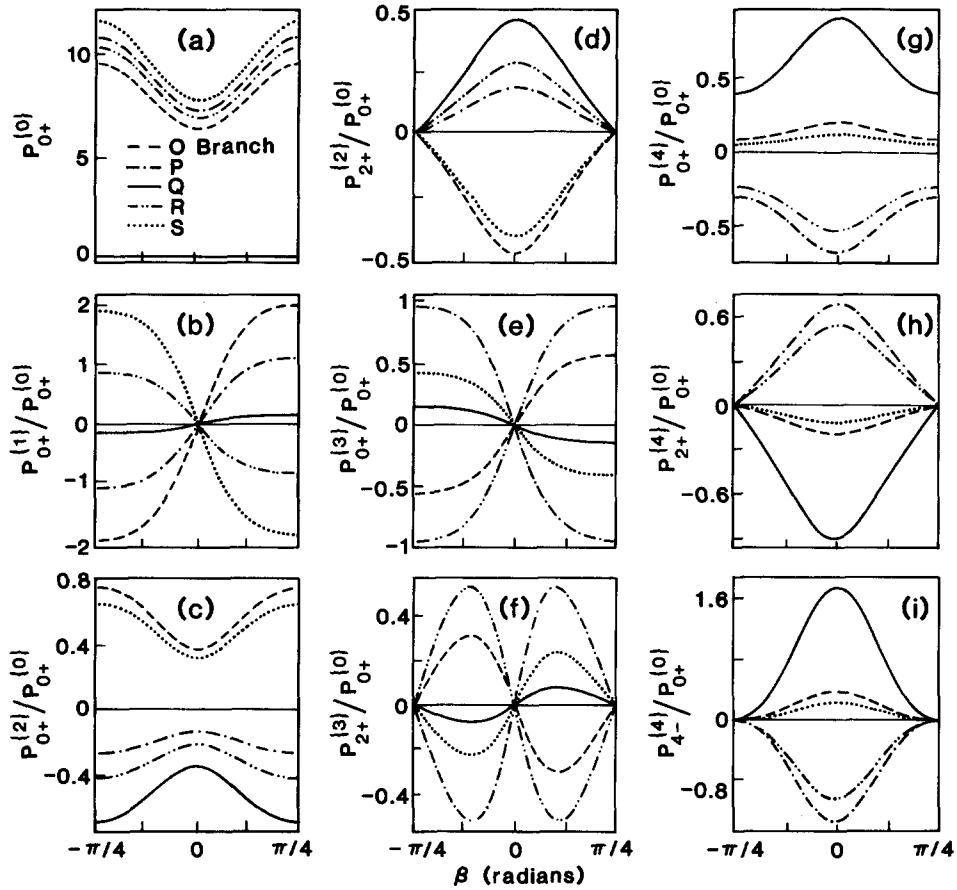

FIG. 4. The moments of the line strength factors $P^{(k)}_{q\pm}$ for case I geometry vs the ellipticity of the radiation β for the five rotational branches of $J_i = 20$ at $\Delta = 22.5°$ in the N_2 $a\,^1\Pi_g$–$X\,^1\Sigma_g^+$ two-photon transition. The higher order moments have been normalized with respect to the zeroth moment. Note: for a given k and q only $P^{(k)}_{q+}$ or $P^{(k)}_{q-}$ is depicted since $P^{(k)}_{q-}(\beta,\Delta) = c(q)\ P^{(k)}_{q+}(\beta,\Delta)$ where $c(q) = -\sin(q\Delta)/\cos(q\Delta)$. We have illustrated the $P^{(k)}_{q+}$ except for $k = 4$ and $q = 4$ since $P^{(4)}_{4+}$ is zero at $\Delta = 22.5°$.

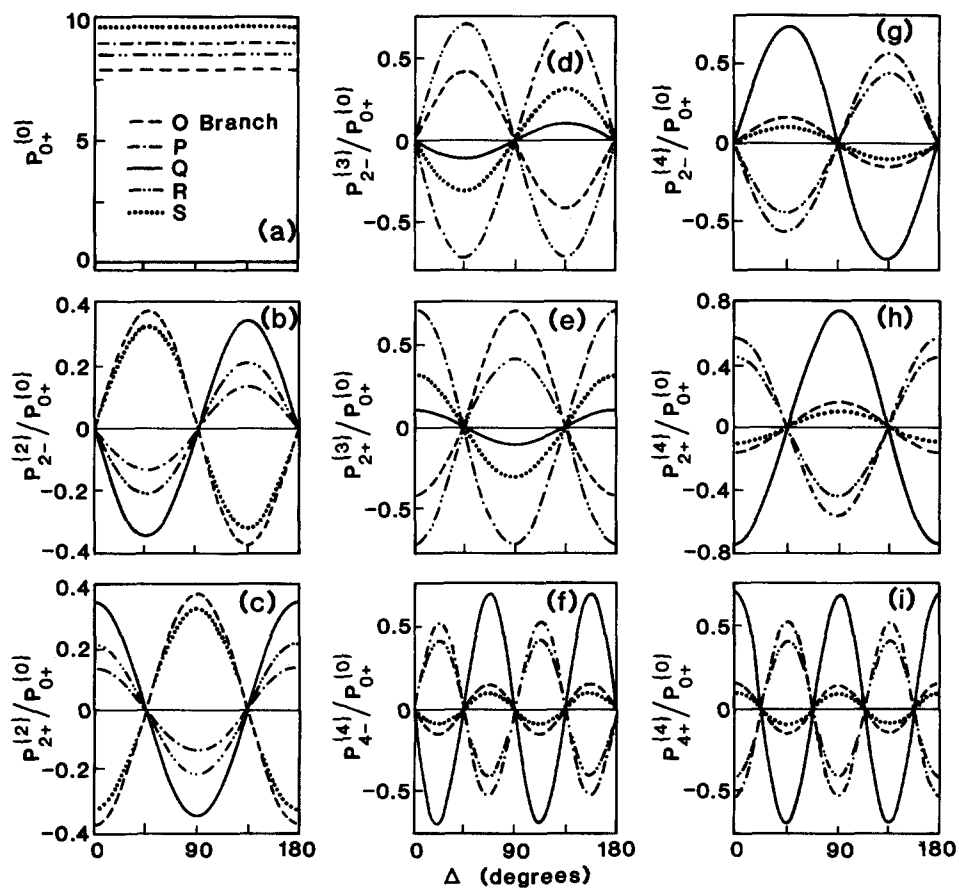

FIG. 5. The moments of the line strength factors $P^{(k)}_{q\pm}$ for case I geometry vs the angle of the major axis of ellipticity of the radiation Δ for the five rotational branches of $J_i = 20$ at $\beta = \pi/8$ in the N_2 $a\,^1\Pi_g$–$X\,^1\Sigma_g^+$ two-photon transition. The higher order moments have been normalized with respect to the zeroth moment. Note: the $P^{(k)}_{0+}/P^{(0)}_{0+}$ are independent of Δ; at $\beta = 22.5°$ for the O, P, Q, R, and S branches $P^{(1)}_{0+} = 13.6,\ 8.49,\ 0.004,\ -6.33,\ -15.8$; $P^{(2)}_{0+} = 4.75,\ -1.93,\ -0.017,\ -2.89,\ 4.99$; $P^{(3)}_{0+} = 3.71,\ -7.24,\ -0.004,\ 6.90,\ -3.37$; and $P^{(4)}_{0+} = 1.01,\ -4.03,\ 0.02,\ -3.01,\ 0.75$.

E. Exploiting the magic angles for case II geometry

If we have a system which has no polarization parameters greater than quadrupole, we can use the magic angles to measure $A_{0+}^{\{0\}}$, $A_{1+}^{\{1\}}$, $A_{1-}^{\{2\}}$, $A_{0+}^{\{2\}}$, and $A_{2+}^{\{2\}}$. First using linearly polarized light ($\beta = 0°$) at $\Delta = 0°$, we compare the intensities from a single J_i measured for two different rotational branches:

$$a_{0+}^{\{0\}} = [I(\Delta = 0°, J_{f1}) - rI(\Delta = 0°, J_{f2})]/ [P_{0+}^{\{0\}}(\Delta = 0°, J_{f1}) - rP_{0+}^{\{0\}}(\Delta = 0°, J_{f2})], \quad (24)$$

$$A_{0+}^{\{2\}} = [I(\Delta = 0°, J_{f2}) - a_{0+}^{\{0\}} P_{0+}^{\{0\}}(\Delta = 0°, J_{f2})]/ [P_{0+}^{\{2\}}(\Delta = 0°, J_{f2}) a_{0+}^{\{0\}}], \quad (25)$$

where

$$r = P_{0+}^{\{2\}}(\Delta = 0°, J_{f1})/P_{0+}^{\{2\}}(\Delta = 0°, J_{f2}). \quad (26)$$

To determine the remaining moments, we need only measure the intensity of one rotational branch with linearly polarized light ($\beta = 0°$) at two magic angles:

$$I'(\Delta = 90°) = I(\Delta = 90°) - [a_{0+}^{\{0\}} P_{0+}^{\{0\}}(\Delta = 90°)] - [a_{0+}^{\{2\}} P_{0+}^{\{2\}}(\Delta = 90°)], \quad (27)$$

$$I'(\Delta = 54.74°) = I(\Delta = 54.74°) - [a_{0+}^{\{0\}} P_{0+}^{\{0\}}(\Delta = 54.74°)] - [a_{2+}^{\{2\}} P_{2+}^{\{2\}}(\Delta = 54.74°)], \quad (28)$$

$$A_{2+}^{\{2\}} = I'(\Delta = 90°)/[P_{2+}^{\{2\}}(\Delta = 90°) a_{0+}^{\{0\}}], \quad (29)$$

$$A_{1-}^{\{2\}} = I'(\Delta = 54.74°)/[P_{1-}^{\{2\}}(\Delta = 54.74°) a_{0+}^{\{0\}}]. \quad (30)$$

In Eqs. (27)–(30), $I'(\Delta)$ is the absorption intensity with the contributions from the $a_{0+}^{\{0\}}$ and $a_{0+}^{\{2\}}$ or $a_{2+}^{\{2\}}$ moments subtracted out. To determine the orientation, at $\Delta = 0°$, we record the intensity of a single rotational line with left and right circularly polarized light:

$$A_{1+}^{\{1\}} = [I(\beta = +45°) - I(\beta = -45°)]/ [2P_{1+}^{\{1\}} a_{0+}^{\{0\}}]. \quad (31)$$

This method measures all five moments with $k \leqslant 2$ which can be detected with case II geometry. However, even if we make multiple measurements at the specified magic angles, we can only calculate standard deviations of the measured polarizations, not their χ^2 values; this is a result of fitting n polarization moments to n unique measurements (in general, n = number of rotational branches probed times the number of angles probed). The value of χ^2 indicates if the data is accurately modeled by the theory while the standard deviations only quantify the scatter in the data. Unfortunately, if χ^2 is not determined, one cannot test whether the two-photon absorption process conforms to the assumptions in this paper or any additional assumptions made by the experimentalist. In order to determine the χ^2, one must fit an overdetermined data set to the theory using, for example, the least-squares techniques described in Secs. III, I–L. The determination of χ^2 can greatly increase the credibility of the measured polarization moments.

F. Detection of alignment and orientation for a system with cylindrical symmetry and case II geometry

If the ground state angular momentum distribution is symmetric about the z axis, there are only three moments which can be detected with case II geometry: $A_{0+}^{\{0\}}$, $A_{0+}^{\{2\}}$, and $A_{0+}^{\{4\}}$. These moments are readily measured; for example, one can use two rotational branches and two magic angles:

$$a_{0+}^{\{0\}} = [I(\Delta = 30.55°, J_{f1}) - rI(\Delta = 30.55°, J_{f2})]/ [P_{0+}^{\{0\}}(\Delta = 30.55°, J_{f1}) - rP_{0+}^{\{0\}}(\Delta = 30.55°, J_{f2})], \quad (32)$$

$$A_{0+}^{\{2\}} = [I(\Delta = 30.55°, J_{f2}) - a_{0+}^{\{0\}} P_{0+}^{\{0\}}(\Delta = 30.55°, J_{f2})]/ [P_{0+}^{\{2\}}(\Delta = 30.55°, J_{f2}) a_{0+}^{\{0\}}], \quad (33)$$

$$A_{0+}^{\{4\}} = [I(\Delta = 54.74°, J_{f2}) - a_{0+}^{\{0\}} P_{0+}^{\{0\}}(\Delta = 54.74°, J_{f2})]/ [P_{0+}^{\{4\}}(\Delta = 54.74°, J_{f2}) a_{0+}^{\{0\}}], \quad (34)$$

where

$$r = P_{0+}^{\{2\}}(\Delta = 30.55°, J_{f1})/P_{0+}^{\{2\}}(\Delta = 30.55°, J_{f2}). \quad (35)$$

Though a system with cylindrical symmetry about the z axis can have two orientation moments, $P_{0+}^{\{1\}}$ and $P_{0+}^{\{3\}}$, these cannot be measured with case II geometry. The advantage in using case II geometry to measure the alignment parameters is that for this geometry the $P_{0+}^{\{k\}}$ vary with Δ and have magic angles while with case I geometry the $P_{0+}^{\{k\}}$ are independent of Δ. The advantage of using case I geometry is that when studying a system with cylindrical symmetry, this geometry is sensitive to the orientation as well as the alignment.

G. Exploiting the magic angles for case III geometry

The magic angles in Δ for the $P_{q\pm}^{\{k\}}$ are identical to those for case II except that the signs have been switched on the components of three line strengths: $P_{1-}^{\{2\}}$ (case II), $P_{1+}^{\{2\}}$ (case III), $P_{1-}^{\{4\}}$ (case II), $P_{1+}^{\{4\}}$ (case III), $P_{3-}^{\{4\}}$ (case II), and $P_{3+}^{\{4\}}$ (case III) have magic angles at $\Delta = 0°$, 90°, and 180°. Consequently, the formulas for case II to determine the polarization parameters for a system with no moments greater than quadrupole [see Eqs. (34–41)] are applicable for case III if we substitute $P_{1+}^{\{2\}}$ for $P_{1-}^{\{2\}}$, $A_{1+}^{\{2\}}$ for $A_{1-}^{\{2\}}$, $P_{1-}^{\{1\}}$ for $P_{1+}^{\{1\}}$, and $A_{1-}^{\{1\}}$ for $A_{1+}^{\{1\}}$.

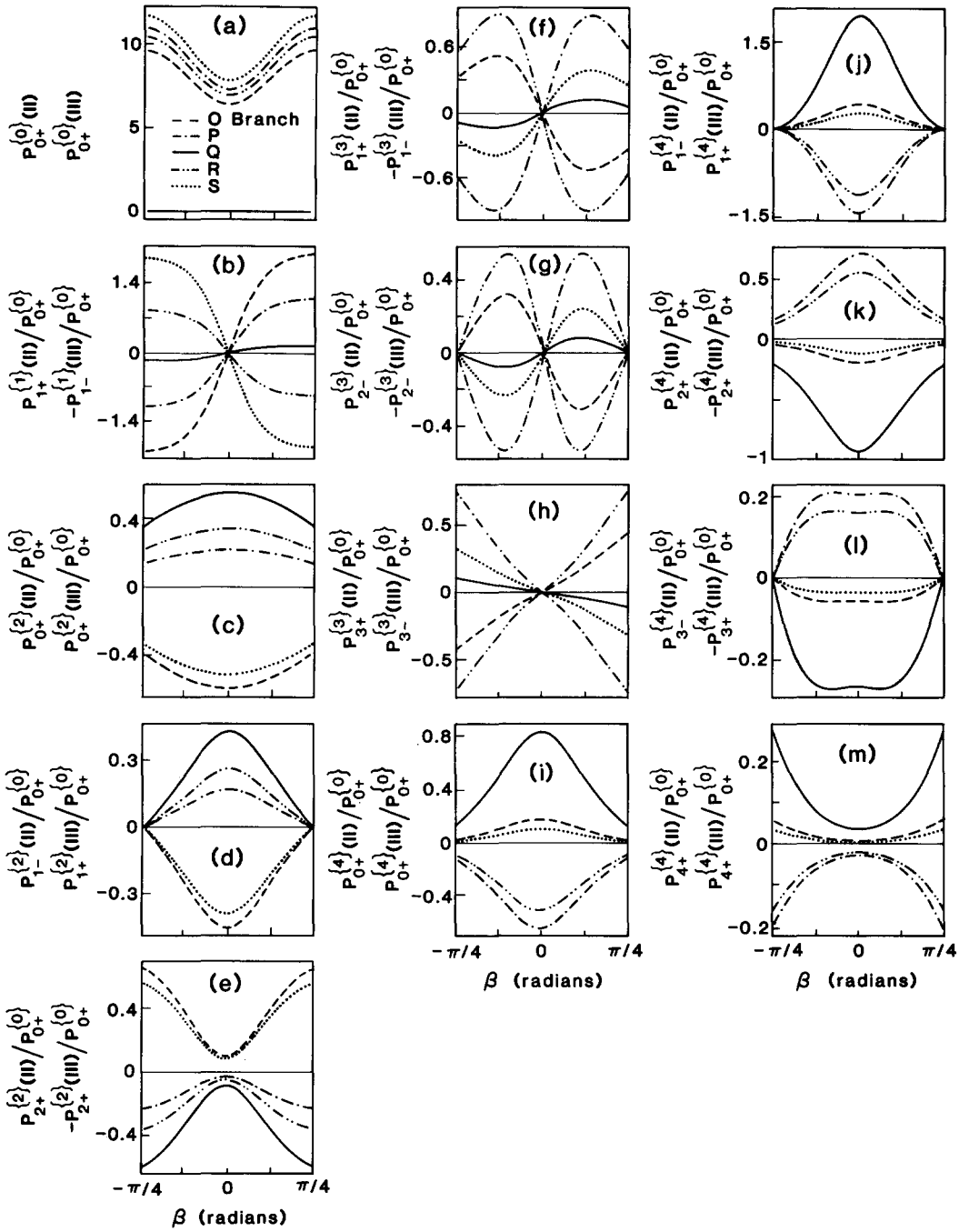

FIG. 6. The moments of the line strength factors $P_{q\pm}^{\{k\}}$ for case II and III geometries vs the ellipticity of the radiation β for the five rotational branches of $J_i = 20$ at $\Delta = 22.5°$ in the N_2 $a\,^1\Pi_g$–$X\,^1\Sigma_g^+$ two-photon transition. The higher order moments have been normalized with respect to the zeroth moment.

H. Detection of alignment and orientation for a system with cylindrical symmetry and case III geometry

Since the magic angles for moments with $q = 0$ are identical for case II and case III geometries, the case II equations which determine the alignment moments for a system possessing cylindrical symmetry about the z axis [see Eqs. (42)–(45)] are equally valid for case III geometry.

I. Determination of the alignment for case I, II, and III geometries

If there are no restrictions on the polarization of the ground state, a detailed measurement for at least three rotational branches of I vs Δ with linearly polarized light $\beta = 0°$ must be performed. Three rotational branches are required because the $P_{q\pm}^{\{k\}}$ do not vary independently with Δ. For example, with case I geometry $P_{0+}^{\{0\}}$, $P_{0+}^{\{2\}}$, and $P_{0+}^{\{4\}}$ are all independent of Δ. Experimentally, variation of Δ is equivalent to rotating the half-wave plate in the absence of the quarter-wave plate. From this data, the alignment moments can be determined using matrix inversion:

$$\vec{I}(J_{fn},\Delta_n) = \mathbf{P}_{q\pm}^{\{k\}}(J_{fn},\Delta_n)\vec{a}_{q\pm}^{\{k\}}, \tag{36a}$$

where

$$n = 0 \rightarrow n_{\max}, \tag{36b}$$

$$(k,q) = (0,0+),\ (2,2-),\ (2,0+),\ (2,2+),\ (4,4-),\ (4,2-),\ (4,0+),\ (4,2+),\ (4,4+)\quad \text{(case I)}, \tag{36c}$$

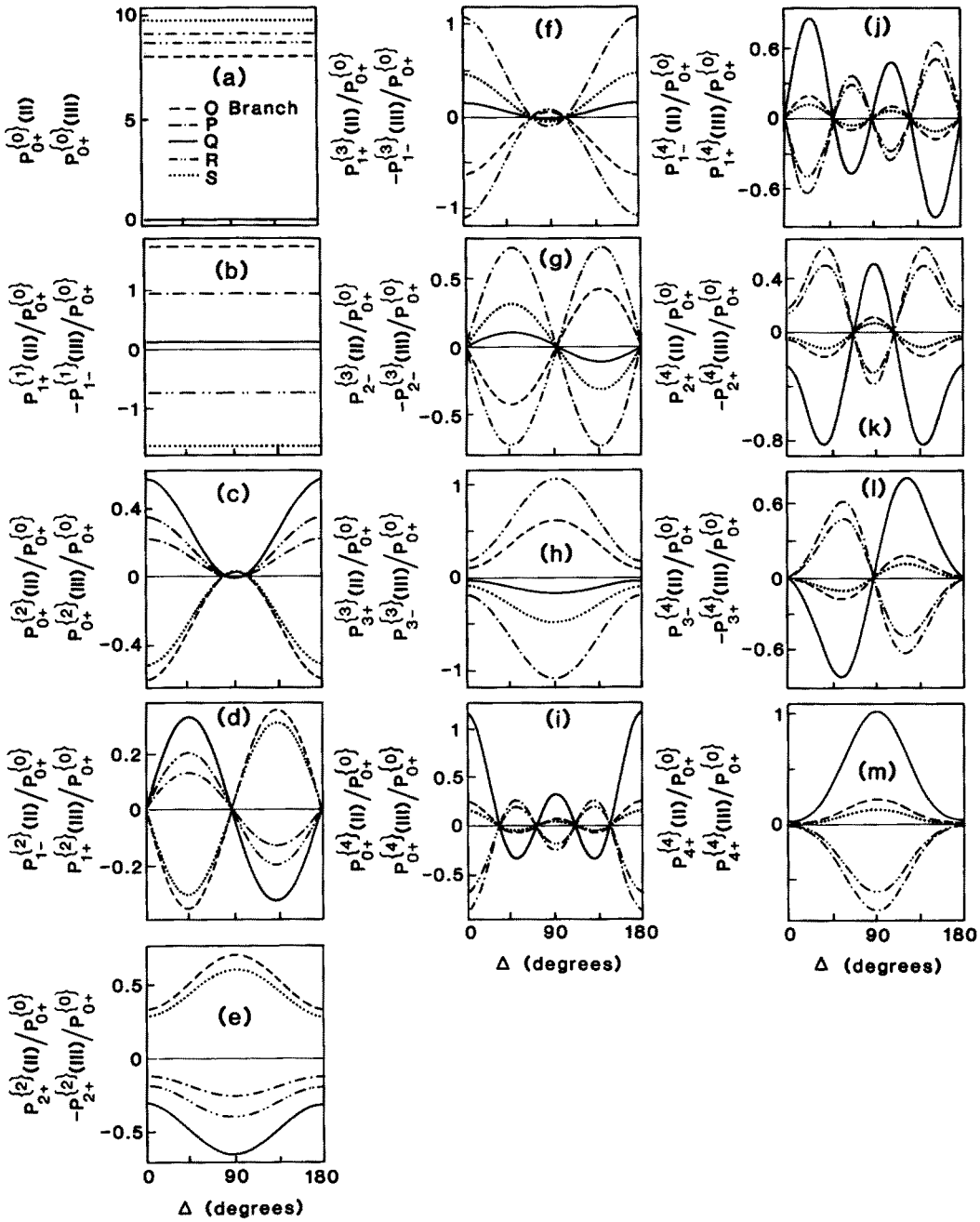

FIG. 7. The moments of the line strength factors $P_{q\pm}^{\{k\}}$ for case II and III geometries vs the angle of the major axis of ellipticity of the radiation, Δ, for the five rotational branches of $J_i = 20$ at $\beta = \pi/8$ in the N_2 $a\,^1\Pi_g - X\,^1\Sigma_g^+$ two-photon transition. The higher order moments have been normalized with respect to the zeroth moment.

$$(k,q) = (0,0+),\ (2,1-),\ (2,0+),\ (2,2+),\ (4,3-),\ (4,1-),\ (4,0+),\ (4,2+),\ (4,4+)\quad \text{(case II)}, \tag{36d}$$

$$(k,q) = (0,0+),\ (2,0+),\ (2,1+),\ (2,2+),\ (4,0+),\ (4,1+),\ (4,2+),\ (4,3+),\ (4,4+)\quad \text{(case III)}. \tag{36e}$$

In Eqs. (36), the subscripts on the angular momentum quantum numbers, J_{fn}, and on the angles, Δ_n, indicate the measurement number. This does not imply that $n_{\max}$ distinct angles need to be measured nor that the intensities from $n_{\max}$ distinct rotational branches need to be recorded. Rather, in general, $n_{\max}/3$ angles would be employed, and at each angle the intensities from three rotational branches would be recorded. We need three independent measurements to differentiate the real polarization moments from the apparent moments (see Table IX).

At first glance, it may appear impossible to extract meaningful values of the alignment parameters using Eqs. (36) because nine parameters are required to fit the data. Two factors may ameliorate this problem. First, if we have some knowledge about how the polarization on the ground state was created, we may be able to assume that several of the alignment and orientation parameters are approximately zero. Second, several of the $a_{q\pm}^{\{k\}}$ (including the $a_{0+}^{\{0\}}$ for all three geometries) have line strengths which are independent of Δ, and hence they may be easy to extract from the data. This is very important because in order to calculate the reduced moments, $A_{q\pm}^{\{k\}}(J_i)$, we must determine $a_{0+}^{\{0\}}(J_i)$.

J. Determination of the apparent alignment polarization moments

Equations (36) require data from three rotational branches for a given J_i; often this may be difficult to obtain. If data are only available from one rotational branch, we cannot determine for a single excitation–detection geometry all the alignment moments, but we can determine the apparent moments which are linear combinations of the alignment moments:

$$A_{q\pm}^{\{k\}}(J_i,J_f)(\text{app}) = \sum_{k'} c(k',q',k,q) \times R(k',q',k,q,J_i,J_f) A_{q'\pm}^{\{k'\}}(J_i,J_f), \tag{37a}$$

$$A_{q\pm}^{\{k\}}(J_i,J_f)(\text{app})/A_{0+}^{\{0\}}(J_i,J_f)(\text{app}) = a_{q\pm}^{\{k\}}(J_i,J_f)(\text{app})/a_{0+}^{\{0\}}(J_i,J_f)(\text{app}), \tag{37b}$$

$$a_{0+}^{\{0\}}(J_i,J_f)(\text{app}) = A_{0+}^{\{0\}}(J_i,J_f)(\text{app}) n(J_i) C(\text{det}), \tag{37c}$$

$$\vec{I}(\Delta_n,J_{f1}) = \mathbf{P}_{\sim q\pm}^{\{k\}}(\Delta_n,J_{f1})\vec{a}_{q\pm}^{\{k\}}(\text{app}), \tag{38a}$$

where

$$n = 0 \rightarrow n_{\max}, \tag{38b}$$

$$(k,q) = (0,0+),\ (2,2-),\ (2,2+),\ (4,4-),\ (4,4+)\quad (\text{case I}), \tag{38c}$$

$$(k,q) = (0,0+),\ (2,1-),\ (2,0+),\ (4,1-),\ (4,0+)\quad (\text{case II}), \tag{38d}$$

$$(k,q) = (0,0+),\ (2,0+),\ (2,1+),\ (4,0+),\ (4,1+)\quad (\text{case III}). \tag{38e}$$

Equations (37a) and (38) seem to imply that the moments of the ground state are not independent. The $A_{q\pm}^{\{k\}}$ and $P_{q\pm}^{\{k\}}$ are independent over all of space, but by varying Δ, we are only probing a single plane of space. By restricting the polarization vector of our linearly polarized light to a single plane, we cause the $P_{q\pm}^{\{k\}}$ to lose their strict independence. The expansion coefficients in Eq. (37a) are specific to each geometry and to $\beta = 0°$. The $c(k',q',k,q)$ are the projections of the parts of the $P_{q'\pm}^{\{k'\}}$ which depend on Δ onto the parts of the $P_{q\pm}^{\{k\}}$ which depend on Δ. The $R(k,q,k'q',J_i,J_f)$ are the projections of the parts of the $P_{q'\pm}^{\{k'\}}$ which are independent of Δ onto the parts of the $P_{q\pm}^{\{k\}}$ which are independent of Δ. These coefficients are derived in the Appendix and are presented in Table IX. Note, as explained in the Appendix, the $A_{q\pm}^{\{k\}}(\text{app})$ are specific to each rotational branch.

It is very important to be aware that even though $A_{0+}^{\{0\}} = 1$, $A_{0+}^{\{0\}}(\text{app})$ is not necessarily unity. Since all the experimentally determined apparent moments have been normalized by $A_{0+}^{\{0\}}(\text{app})$, when comparing theoretically determined apparent moments (for example, from trajectory calculations) with experimentally determined apparent moments, the theoretically calculated moments should be divided by $A_{0+}^{\{0\}}(\text{app})$. This is also true for the population, $n(J_i)\cdot C(\text{det})$; in general, for a given excitation–detection geometry, the experimentalist cannot exactly determine the rotational populations, only $A_{0+}^{\{0\}}(\text{app})\, n(J_i)\, C(\text{det})$.

K. Determination of the orientation for case I, II, and III geometries

To determine the orientation, we change the degree of ellipticity, β, while keeping the angle Δ between x_d and the major axis of the polarization ellipsoid fixed. Experimentally, the half-wave plate is rotated while the position of the quarter-wave plate is kept constant. The recorded intensities are fitted to all the line strengths:

$$\vec{I}(J_{fn},\beta_n) = \mathbf{P}_{\sim q\pm}^{\{k\}}(J_{fn},\beta_n)\vec{a}_{q\pm}^{\{k\}}(J_i,J_f)(\text{app}), \tag{39a}$$

where

$$n = 0 \rightarrow n_{\max}. \tag{39b}$$

For case I:

$$(k,q) = (0,0+),\ (1,0+),\ (2,0+),\ (3,2-),\ (3,0+),\ (3,2+),\ (4,0+);$$
$$a_{0+}^{\{0\}}(\text{app}) = f[a_{0+}^{\{0\}}, a_{2-}^{\{2\}}, a_{2+}^{\{2\}}, a_{4-}^{\{4\}}, a_{2-}^{\{4\}}, a_{2+}^{\{4\}}, a_{4+}^{\{4\}}];$$
$$a_{0+}^{\{2\}}(\text{app}) = f[a_{0+}^{\{2\}}, a_{2-}^{\{2\}}, a_{2+}^{\{2\}}, a_{4-}^{\{4\}}, a_{2-}^{\{4\}}, a_{2+}^{\{4\}}, a_{4+}^{\{4\}}];$$
$$a_{0+}^{\{4\}}(\text{app}) = f[a_{0+}^{\{4\}}, a_{2-}^{\{2\}}, a_{2+}^{\{2\}}, a_{4-}^{\{4\}}, a_{2-}^{\{4\}}, a_{2+}^{\{4\}}, a_{4+}^{\{4\}}];$$
$$a_{1-}^{\{1\}}(\text{app}) = a_{1-}^{\{1\}};\ a_{2-}^{\{3\}}(\text{app}) = a_{2-}^{\{3\}};\ a_{0+}^{\{3\}}(\text{app}) = a_{0+}^{\{3\}};\ a_{2+}^{\{3\}}(\text{app}) = a_{2+}^{\{3\}}. \tag{39c}$$

For case II:

$$(k,q) = (0,0+),\ (1,1+),\ (2,0+),\ (3,1+),\ (3,2-),\ (3,3+),\ (4,0+);$$
$$a_{0+}^{\{0\}}(\text{app}) = f[a_{0+}^{\{0\}}, a_{1-}^{\{2\}}, a_{2+}^{\{2\}}, a_{1-}^{\{4\}}, a_{2+}^{\{4\}}, a_{3-}^{\{4\}}, a_{4+}^{\{4\}}];$$
$$a_{0+}^{\{2\}}(\text{app}) = f[a_{0+}^{\{2\}}, a_{1-}^{\{2\}}, a_{2+}^{\{2\}}, a_{1-}^{\{4\}}, a_{2+}^{\{4\}}, a_{3-}^{\{4\}}, a_{4+}^{\{4\}}];$$
$$a_{0+}^{\{4\}}(\text{app}) = f[a_{0+}^{\{4\}}, a_{1-}^{\{2\}}, a_{2+}^{\{2\}}, a_{1-}^{\{4\}}, a_{2+}^{\{4\}}, a_{3-}^{\{4\}}, a_{4+}^{\{4\}}];$$
$$a_{1+}^{\{1\}}(\text{app}) = a_{1+}^{\{1\}};\ a_{1+}^{\{3\}}(\text{app}) = a_{1+}^{\{3\}};\ a_{2-}^{\{3\}}(\text{app}) = a_{2-}^{\{3\}};\ a_{3-}^{\{3\}}(\text{app}) = a_{3-}^{\{3\}}. \tag{39d}$$

For case III:

$$(k,q) = (0,0+),\ (1,1-),\ (2,0+),\ (3,1-),\ (3,2-),\ (3,3-),\ (4,0+);$$
$$a_{0+}^{\{0\}}(\text{app}) = f[a_{0+}^{\{0\}}, a_{1+}^{\{2\}}, a_{2+}^{\{2\}}, a_{1+}^{\{4\}}, a_{2+}^{\{4\}}, a_{3+}^{\{4\}}, a_{4+}^{\{4\}}];$$
$$a_{0+}^{\{2\}}(\text{app}) = f[a_{0+}^{\{2\}}, a_{1+}^{\{2\}}, a_{2+}^{\{2\}}, a_{1+}^{\{4\}}, a_{2+}^{\{4\}}, a_{3+}^{\{4\}}, a_{4+}^{\{4\}}];$$
$$a_{0+}^{\{4\}}(\text{app}) = f[a_{0+}^{\{4\}}, a_{1+}^{\{2\}}, a_{2+}^{\{2\}}, a_{1+}^{\{4\}}, a_{2+}^{\{4\}}, a_{3+}^{\{4\}}, a_{4+}^{\{4\}}];$$
$$a_{1-}^{\{1\}}(\text{app}) = a_{1-}^{\{1\}};\ a_{1-}^{\{3\}}(\text{app}) = a_{1-}^{\{3\}};\ a_{2-}^{\{3\}}(\text{app}) = a_{2-}^{\{3\}};\ a_{3-}^{\{3\}}(\text{app}) = a_{3-}^{\{3\}}. \tag{39e}$$

Note that for an orientation measurement we directly determine all the orientation moments, but we only measure apparent alignment moments. The definitions of the apparent moments for an orientation measurement are different than those for an alignment measurement; consequently, we cannot use Table IX for orientation measurements; instead we must use Eq. (A23) to numerically calculate the expansion coefficient for the definitions of the apparent moments. In general it is advantageous to do orientation measurements at $\Delta = 0°$ since the line strengths of many of the moments are zero at this angle; this greatly simplifies the definitions of the apparent moments (see Figs. 5 and 7).

If we were to measure intensity versus ellipticity (I vs β) for several values of "delta" (this rotates the direction of the major axis of elliptical polarization), then we could determine the real moments instead of the apparent moments. In general, it is not necessary to record I vs β at several Δ since when performing orientation measurements we just want to determine the orientation moments, and they are only affected by the apparent moments through their normalization with respect to $a_{0+}^{\{0\}}$ (app); see Eq. (37b).

Directly fitting data taken with elliptically polarized light to the alignment and orientation parameters allows the simultaneous determination of the $a_{q\pm}^{\{k\}}$ and $a_{0+}^{\{0\}}$ and hence the determination of the unreduced moments. Unfortunately, the variation of the $P_{0+}^{\{0\}}$, $P_{q\pm}^{\{2\}}$, and $P_{q\pm}^{\{4\}}$ with β are similar; hence, it is difficult to determine the alignment moments or the populations using this method. To determine the alignment moments and the population, a measurement of I vs Δ at $\beta = 0°$ should be performed.

It is most convenient to record the intensity at pairs of angles, $+\beta$ and $-\beta$; subtracting the two intensities gives us "delta intensity" $\Delta I(\beta) = \{I(+\beta) - I(-\beta)\}/2$, which is independent of the alignment since all the alignment moments have line strengths which are identical at $\pm\beta$:

$$\Delta\vec{I}(J_{fn},\beta_n) = \underset{\sim}{\mathbf{P}}_{q\pm}^{\{k\}}(J_{fn},\beta_n)\vec{a}_{q\pm}^{\{k\}}, \tag{40a}$$

where

$$n = 0 \rightarrow n_{\max}, \tag{40b}$$

$$(k,q) = (1,0+),\ (3,2-),\ (3,0+),\ (3,2+)\quad \text{(case I)}, \tag{40c}$$

$$(k,q) = (1,1+),\ (3,2-),\ (3,1+),\ (3,3+)\quad \text{(case II)}, \tag{40d}$$

$$(k,q) = (1,1-),\ (3,3-),\ (3,2-),\ (3,1-)\quad \text{(case III)}. \tag{40e}$$

L. Determination of the octupole orientation polarization moments

If only one rotational branch is being probed, it may be difficult to differentiate between the contributions from the different orientation moments. When there is a small amount of orientation, it would be particularly difficult to measure the octupole moments using Eqs. (40) since the contributions from the octupole moments may be masked by the contribution from the dipole moment. There is a better way to detect at least two of the octupole moments: for a fixed ellipticity β, record ΔI of a single rotational line as a function of Δ, and calculate $\delta I(\Delta)$ and $\delta P(\Delta)$:

$$\delta I(\Delta_n) = [I(+\beta,\Delta_n) - I(-\beta,\Delta_n)]/2 - [I(+\beta,\Delta = 0°) - I(-\beta,\Delta = 0°)]/2, \tag{41}$$

$$\delta P_{q\pm}^{\{k\}}(\Delta_n) = P_{q\pm}^{\{k\}}(+\beta,\Delta_n) - P_{q\pm}^{\{k\}}(+\beta,\Delta = 0°), \tag{42}$$

$$\delta\vec{I}(J_{fn},\beta_n) = \delta\underset{\sim}{\mathbf{P}}_{q\pm}^{\{k\}}(J_{fn},\beta_n)\vec{a}_{q\pm}^{\{k\}}, \tag{43a}$$

where

$$n = 0 \rightarrow n_{\max}, \tag{43b}$$

$$(k,q) = (3,2-),\ (3,2+)\quad \text{(case I)}, \tag{43c}$$

$$(k,q) = (3,2-),\ (3,1+),\ (3,3+)\quad \text{(case II)}, \tag{43d}$$

$$(k,q) = (3,3-),\ (3,2-),\ (3,1-)\quad \text{(case III)}. \tag{43e}$$

Using these Eqs. (41)–(43) two or three octupole moments can be determined [$a_{2-}^{\{3\}}$ (case I), $a_{2+}^{\{3\}}$ (case I)], [$a_{1+}^{\{3\}}$ (case II), $a_{2-}^{\{3\}}$ (case II), $a_{3+}^{\{3\}}$ (case II)], and [$a_{1-}^{\{3\}}$ (case III), $a_{2-}^{\{3\}}$ (case III), $a_{3-}^{\{3\}}$ (case III)]. After these moments have been determined, we can fit the data of I vs β using just one or two parameters to determine the remaining orientation moments [$a_{0+}^{\{1\}}$ (case I), $a_{0+}^{\{3\}}$ (case I)], [$a_{1+}^{\{1\}}$ (case II)], and [$a_{1-}^{\{1\}}$ (case III)]:

$$\delta\vec{I}'(J_{fn},\beta_n) = \underset{\sim}{\mathbf{P}}_{q'\pm}^{\{k'\}}(J_{fn},\beta_n)\vec{a}_{q'\pm}^{\{k'\}}, \tag{44a}$$

where

$$\delta I'(\beta) = [\Delta I(+\beta) - \Delta I(-\beta)]/2 - \sum_{k,q} a_{q\pm}^{\{k\}} P_{q\pm}^{\{k\}}(+\beta), \tag{44b}$$

$$n = 0 \rightarrow n_{\max}, \tag{44c}$$

$$(k',q') = (1,0+),\ (3,0+)\quad \text{(case I)}, \tag{44d}$$

$$(k',q') = (1,1+)\quad \text{(case II)}, \tag{44e}$$

$$(k',q') = (1,0-)\quad \text{(case III)}, \tag{44f}$$

and k and q are defined in Eqs. (40c)–(40e). Equations (43) and (44a) will determine the orientation moments more accurately than Eqs. (40) since the former employ fewer fitting parameters. All these equations determine only the unreduced moments of the orientation; in order to determine the reduced moments, the population must be calculated using Eq. (19). Even when the population has not been determined, Eqs. (43) and (44) yield accurate ratios of the reduced moments since

$$A_{q\pm}^{\{k\}}/A_{q'\pm}^{\{k'\}} = a_{q\pm}^{\{k\}}/a_{q'\pm}^{\{k'\}}. \tag{45}$$

IV. POLAR PLOTS OF THE PURE MOMENTS OF A DISTRIBUTION

We want to derive equations which will depict the shapes of the alignments and orientation moments in the high J_i limit. This was already done in KSZ for the moments which can be detected with linearly polarized light and case III geometry. Unfortunately, the nomenclature used for this

calculation in KSZ cannot be readily extended to include all the orientation and alignment moments so we will rederive the equation for the three-dimensional probability distribution, $P(J,M_x,M_y,M_z)$. We will define the real moments $A_{q\pm}^{\{k\}}$ as

$$A_{q\pm}^{\{k\}}(J) = c(k)\langle (J_iM_i\Lambda_i|J_{q\pm}^{\{k\}}|J_iM_i\Lambda_i\rangle / [(J_iM_i\Lambda_i|\mathbf{J}^2|J_iM_i\Lambda_i)]^{k/2}. \quad (46)$$

The normalization constant, $c(k)$, has been assigned by GZ for $k = 0,2$, and 4, but we are free to choose the values for $k = 1,3$. We will choose the values of $c(k)$ for $k = 1,3$ so that the $A_{0+}^{\{k\}}$ equals the corresponding Legendre polynomial $P_k[\cos(J_z/\mathbf{J})]$ in the high J limit. This formula will also work for the established values of $c(k=0)$ and $c(k=4)$, but will give a normalization constant for $k = 2$ which is only one-half the established value:

$$c(k\neq 2) = \{P_k(\cos\theta)[(J_iM_i\Lambda_i|\mathbf{J}^2|J_iM_i\Lambda_i)]^{k/2} / \langle (J_iM_i\Lambda_i|J_{q\pm}^{\{k\}}|J_iM_i\Lambda_i)\rangle\}_{J\to\infty}, \quad (47)$$

where

$$\cos\theta = \{M_z/[J(J+1)]^{1/2}\}_{J\to\infty}. \quad (48)$$

The values of $c(k)$ are listed in Table IV. In Eq. (46), the magnetic quantum numbers "M" refer to all the magnetic quantum numbers, M_x, M_y, M_z which are the expectation values of the operators J_x, J_y, and J_z. This does not imply that we can measure these quantities simultaneously, but rather that for an ensemble of molecules we can independently measure the expectation values of each magnetic quantum number (or the expectation values of multiples of the magnetic quantum numbers). For example, we could measure the spectrum of an ensemble first with a Stark field along the x axis, then with a Stark field along the y axis, and finally with a Stark field along the z axis. We denote the measured populations in these three experiments as $P(J,M_x)$, $P(J,M_y)$, and $P(J,M_z)$. These are the probabilities of a molecule in rotational state J being found in M_x, M_y, or M_z. We define $P(J,M) = P(J,M_x,M_y,M_z) = P(J,M_x)\,P(J,M_y)\,P(J,M_z)$. [Note in KSZ1 we refered to $P(J,M_x,M_y,M_z)$ as $P(J,J_x,J_y,J_z)$; this is a misnomer since the J_x, J_y, and J_z are operators not expectation values.] A quantum mechanical or classical theoretical calculation can also predict these independent expectation values. To compare experimental results with theory, the polarization moments of a theoretical calculation can be computed with Eq. (46).

To calculate the three-dimensional probability distribution in terms of the real tensor operators, we first express $A_q^k(J)$ in terms of $P(J,M_x,M_y,M_z)$ using the complex tensor operators:

$$A_q^k(J) = \frac{c(k)(JM|\mathbf{J}^2|JM)^{-k/2}\Sigma_{M_x,M_y,M_z} P(J,M_x,M_y,M_z)(JM|J_q^{(k)}|JM)}{\Sigma_{M_x,M_y,M_z} P(J,M_x,M_y,M_z)}. \quad (49a)$$

We solve Eq. (49a) for $P(J,M_x,M_y,M_z)$ by multiplying both sides by $\Sigma_{k,q}(2k+1)(JM'|J_q^{(k)}|JM')/(J||J^{(k)}||J)^2$ and noting that the sum of $P(J,M_x,M_y,M_z)$ over all M_x,M_y,M_z is the population $n(J)$ of level J:

$$n(J)\sum_{k,q} A_q^k(2k+1)(JM|\mathbf{J}^2|JM)^{k/2}(JM'|J_q^{(k)}|JM')/[c(k)(J||J^{(k)}||J)^2] = \sum_{M_x,M_y,M_z} P(J,M_x,M_y,M_z)\sum_{k,q}(2k+1)(J||J^{(k)}||J)^{-2}(JM'|J_q^{(k)}|JM')(JM|J_q^{(k)}|JM). \quad (49b)$$

Application of the Wigner–Eckart theorem [see Eq. (5.4.1) of Edmonds[18]] to both matrix elements on the right-hand side of Eq. (49b) and the orthonormality of the resulting $3-j$ symbols [see Eq. (3.7.7) of Edmonds[18]] gives

$$P(J_i,M_x,M_y,M_z) = n(J_i)\sum_{k,q}\xi(J_i,k)A_q^k(J_i)(J_iM_i|J_q^{(k)}|J_iM_i), \quad (49c)$$

where

$$\xi(J,K) = (2k+1)[J(J+1)]^{k/2}/[c(k)(J||J^{(k)}||J)^2], = (2k+1)c(k)[b^k(J)]^2/[J(J+1)]^{k/2}. \quad (50)$$

In Eq. (49c), we have omitted the orbital angular momentum quantum numbers Λ_i for the sake of brevity. Using, Eq. (A49) of KSZ, we convert the tensors in Eq. (49) to the Hertel–Stoll normalization:

$$P(J_i,M_x,M_y,M_z) = n(J_i)\sum_{k,q}\xi(J_i,k)[A_{q+}^{\{k\}}(J_i)(J_iM_i|J_{q+}^{\{k\}}|J_iM_i) - A_{q-}^{\{k\}}(J_i)(J_iM_i|J_{q-}^{\{k\}}|J_iM_i)]. \quad (51)$$

The sum over k ranges from 0 to $2J$ and q ranges from 0 to k. However, with two-photon excitation, we can only detect $k\leqslant 4$ so we can never completely determine the $|JM\rangle$ distribution for $J>2$. However, we can depict the angular momentum distribution if we ignore all moments that we cannot measure, or we can depict a distribution of any single moment.

In the high J limit the expectation values of the angular momentum spherical tensor operators are proportional to the spherical harmonics multiplied by normalization constants, $c(k)$ and $v(k)$, and the reduced matrix elements of the angular momentum spherical tensor operators, $b(k)$:

$$v(k) = \{[J_{q\pm}^{\{k\}}/(J(J+1))^{k/2}]/Y_{q\pm}^{\{k\}}(\theta,\phi)\}_{J\to\infty}, \quad (52)$$

$$P(J,M_x,M_y,M_z)$$

$$= n(J) \sum_{k,q} (2k+1)[b^k(J)]^2 c(k) v(k) \times [A^{\{k\}}_{q+}(J) Y^{\{k\}}_{q+}(\theta,\phi) - A^{\{k\}}_{q-}(J) Y^{\{k\}}_{q-}(\theta,\phi)], \quad (53)$$

where

$$\cos\theta = J_z/(J_x^2 + J_y^2 + J_z^2)^{1/2}, \quad (54)$$

$$\sin\theta\cos\phi = J_x/(J_x^2 + J_y^2 + J^2)^{1/2}, \quad (55)$$

$$\sin\theta\sin\phi = J_y/(J_x^2 + J_y^2 + J_z^2)^{1/2}. \quad (56)$$

The $v(k)$ are tabulated in Table IV. The $Y^{\{k\}}_{q\pm}$ are the spherical harmonic functions in the Hertel–Stoll normalization. They are generated from the standard spherical harmonics using Eqs. (A6) and (A7).

The shapes of all the polarization moments in the high J limit (the spherical harmonics) for $k \leqslant 4$ can be found in Figs. 7 and 8 of KSZ and Fig. 8 of this paper. The moments depicted in KSZ are the $(-1)^q A^{\{k\}}_{q+}$ with even ranks while those in Fig. 8 of this paper are the $A^{\{k\}}_{q+}$ with odd ranks. The shapes of the $A^{\{k\}}_{q-}$ can be determined from the shapes of the $A^{\{k\}}_{q+}$ by rotating the x–y plane by $(90°/q)$ while keeping the figure of $A^{\{k\}}_{q+}$ fixed.

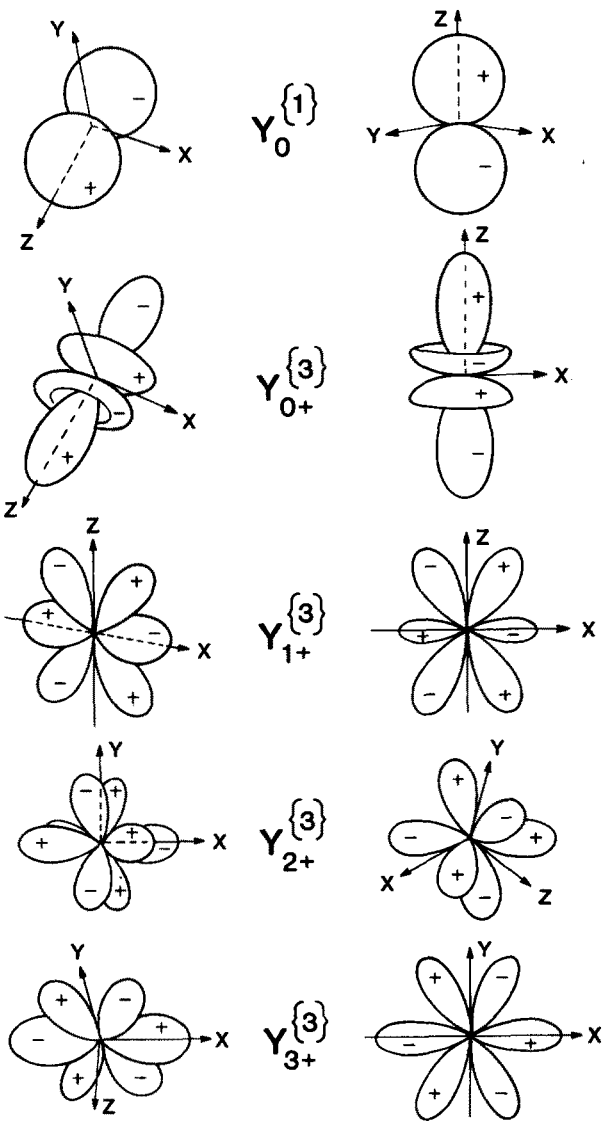

FIG. 8. Three-dimensional diagrams of the $A^{\{k\}}_{q+}(J_i)$ with odd ranks in the high J_i limit. The $A^{\{k\}}_{q-}(J_i)$ can be generated from the $A^{\{k\}}_{q+}(J_i)$ by relabeling the axes by rotating the x–y plane by $(90°/q)$ while keeping the figure of $A^{\{k\}}_{q+}$ constant. $Y^{\{1\}}_{1+}$ is generated from $Y^{\{1\}}_{0+}$ by interchanging the z and $-x$ axes. These plotted functions are proportional to the corresponding real spherical harmonics, $Y^{\{k\}}_{q\pm}$.

To determine if a given orientation can be detected for a particular laser propagation axis, this axis must be drawn to intersect the origin of an orientation moment. If the axis hits lobes of opposite sign on either side of the origin then that moment can be detected with elliptically polarized light propagating along the axis as drawn.

To determine if a given laser geometry can detect an alignment moment, the laser propagation axis is drawn through the origin of the alignment moment, and the electric field vector of the linearly polarized light is drawn perpendicular to this axis. If the net projection of the electric field vector on all the lobes of the alignment moments is nonzero when the alignment of this moment can be detected with the given detection geometry.

One last note: we can combine Eqs. (46) and (52) to arrive at a definition of the $A^{\{k\}}_{q\pm}$ in the high J limit: $A^{\{k\}}_{q\pm} = c(k)v(k)\langle|Y^{\{k\}}_{q\pm}|\rangle$. This definition could be useful when calculating the polarization moments for a given distribution, such as that produced from classical trajectory calculations.

V. TYPES OF ELLIPTICALLY POLARIZED LIGHT

The calculation of the line strengths has assumed that the light is monochromatic and coherent and that the elliptical polarization has been produced with a quarter-wave plate. The latter requirement is easy to fulfill, and we will explain why it is imperative to use a quarter-wave plate by calculating the line strengths for a variable shift wave plate, for example a one-fifth-wave plate. Most pulsed dye lasers do not produce a single-mode Fourier transform limited bandwidth output, and we will explain how this could only affect the absolute magnitudes of the radial terms.

A. Variable phase shift wave plates

By "variable phase shift wave plate" we mean a device which creates a stable phase shift other than $\pi/4$; for example a nonquarter-wave plate or Soleil–Babinet compensator. To include the effect of a variable phase shift wave plate, we need to calculate the electric field vector cross products, E^k_q, under the assumption that the wave plate induces a relative phase shift of ξ between the components of the electric field vector of the light lying along the major and minor axes of the wave plate. This has been done in the Appendix, and the results are tabulated in Table III.

Figure 9 is a plot of $P^{\{k\}}_{q\pm}$ vs β, for $J_i = 20$, $\xi = 105.0°$, and $\Delta = 22.5°$ for the $a\,^1\Pi_g$–$X\,^1\Sigma_g^+$ excitation of N_2. This is the same case as given in Sec. IV. Figures 7 and 9 can be directly compared to assess the effect of using a variable wave plate. Note that a quarter-wave plate corresponds to $\xi = 90°$. For $\xi \neq 90°$, all the octupole orientation moments are no longer asymmetric about $\beta = 0°$. For example, in Fig. 9, $P^{\{3\}}_{1-}$ has a magnitude which is double at $\beta = +45°$ vs $\beta = -45°$. More importantly, for $\xi \neq 90°$ the alignments

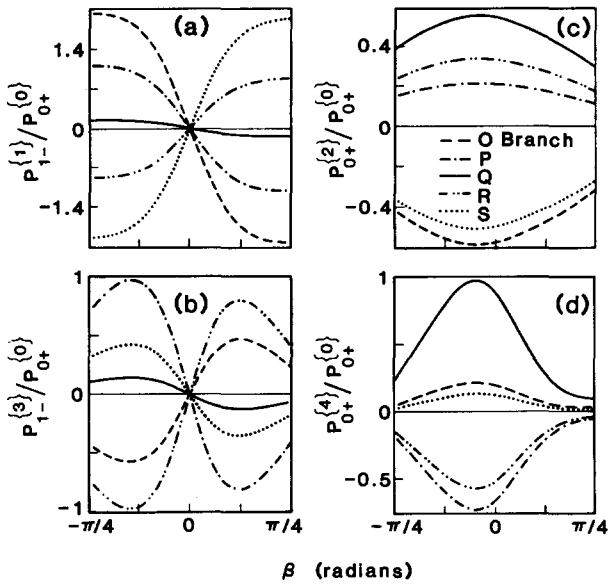

FIG. 9. Effects of using a variable phase shift wave plate (nonquarter-wave plate) upon $P_{q\pm}^{(k)}$ vs the angle of the major axis of ellipticity of the radiation Δ for case III geometry. The five rotational branches of $J_i = 20$ are depicted for $\beta = \pi/8$ and $\xi = 7\pi/12$ ($\xi' = -15°$), in the N_2 $a\,^1\Pi_g$–$X\,^1\Sigma_g^+$ two-photon transition. The higher order moments have been normalized with respect to the zeroth moment.

moments are no longer symmetric about $\beta = 0°$. For example, in Fig. 9, $P_{0+}^{\{2\}}$ is 50% larger at $\beta = +45°$ than at $\beta = -45°$.

Since we can calculate the line strengths for any given phase shift, ξ, we can analyze data taken with a variable phase shift device. However, if we are not using a quarter-wave plate, $\xi \neq 90°$, then $\Delta I = I(+\beta) - I(-\beta)$ is no longer just a function of the orientation moments. This is very important experimentally because if a "bad" quarter-wave plate is used to measure nonzero values of ΔI, the system may only possess alignment even though one might conclude orientation is present.

B. Effects of incoherence

In this calculation we have assumed that "pure elliptically polarized light" (PEPL) is employed for the multiphoton absorption. By PEPL we mean light that has been created by passing a laser pulse of Fourier-transform limited bandwidth, single longitudinal mode light through quarter- and half-wave plates. This light is special because it is coherent both in the near and far fields.

If a laser pulse contains more than one mode, the modes can interfere and raise or lower the observed intensity from a multiphoton absorption. If the bandwidth of the laser is greater than the Fourier-transform limit then, in the far field, the red side of the laser pulse will be out of phase with the blue side of the laser pulse. This can result in interference effects which change the observed intensity from a multiphoton process.

Having laser light which is not PEPL does not matter so long as the laser pulses do not have stable, repeatable internal coherences. First, the phase relationships between the various modes in the laser pulse should be random when averaged over many laser shots. Second, if each mode is much wider than the Fourier-transform limit, the multiphoton process should occur in the far field where the phase relationship between the red and blue sides of the bandwidth is random when averaged over many laser shots.

In sum, in order to use these equations, we must either employ PEPL or pulsed laser light which then averaged over many laser shots behaves as PEPL but with a different efficiency for multiphoton absorption.

VI. ABSORPTION PROBABILITIES FOR SPECIFIC $|J_iM_i\rangle$ STATES

We can understand why the S and R rotational branches have dipole line strengths of opposite sign to the O and P rotational branches by calculating the absorption probabilities for single $|J_iM_i\rangle$ states, $I(J_i,M_i)$. The equation for $I(J_i,M_i)$ along with some physical insight allows us to deduce the direction of rotation for a molecule whose S branch transition is enhanced by circularly polarized light.

To calculate $I(J_i,M_i)$ we sum the transition amplitudes over all possible J_e and Λ_e but with a fixed M_i. Since we will be using circularly or linearly polarized light, M_e,M_f are also fixed:

$$I(J_i,M_i) = \Bigg(\sum_{J_e\Lambda_e\gamma_e} (J_f,M_f,\Lambda_f|\boldsymbol{\mu}\cdot\boldsymbol{\epsilon}|J_e,M_e,\Lambda_e,\gamma_e) \times (J_e,M_e,\Lambda_e,\gamma_e|\boldsymbol{\mu}\cdot\boldsymbol{\epsilon}|J_i,M_i,\Lambda_i) \times [E_{ei} - h\nu + i(\Gamma_e/2)]^{-1} \Bigg)^2, \tag{57}$$

$$\boldsymbol{\mu}\cdot\boldsymbol{\epsilon} = \sum_s \mathbf{r}_s\cdot\boldsymbol{\epsilon} = (4\pi/3)^{1/2} \sum_s r_s Y_u^{(1)}(\hat{\mathbf{r}}_{\text{space}}). \tag{58}$$

In Eq. (58), the component of the spherical harmonic indicates the type of light used for excitation: $u = 0$ for light linearly polarized along the z axis and $u = \pm 1$ for circularly polarized light propagating along the y axis. Using methods identical to those in Eqs. (A20)–(A25) of KSZ and Eqs. (4.2.7) and (4.6.2) of Edmonds[18]:

$$I(J_i,M_i) = (4\pi/3)^2 \Bigg[[(2J_i+1)(2J_f+1)]^{1/2} \sum_{J_e\Lambda_e} (-1)^{(u+\Lambda_e-\Lambda_f)} (2J_e+1) R_{ei}^{\Lambda_e-\Lambda_i} R_{fe}^{\Lambda_f-\Lambda_e} \times \begin{pmatrix} J_e & 1 & J_i \\ M_e & -u & -M_i \end{pmatrix} \begin{pmatrix} J_e & 1 & J_i \\ \Lambda_e & \Lambda_i-\Lambda_e & -\Lambda_i \end{pmatrix} \begin{pmatrix} J_f & 1 & J_e \\ M_f & -u & -M_e \end{pmatrix} \begin{pmatrix} J_f & 1 & J_e \\ \Lambda_f & \Lambda_e-\Lambda_f & -\Lambda_e \end{pmatrix} \Bigg]^2 \tag{59}$$

and the total radial parts of the transition $R_{21}^{\Delta\Lambda}$ are defined in Eqs. (A24b) and (A24c) of KSZ. The radial terms are not important since we are only interested in the relative $I(J_i,M_i)$ for different M_i so we set them equal to unity in subsequent calculations. Very similar equations have been derived by Dixit and McKoy,[19] but they used a nonconventional phase convention on their rotational wave functions [see Eq. (2) of Dixit and McKoy[19] and Eq. (A21) of KSZ].

Note that Eq. (A24a) of KSZ is missing the sum over the positions of the electrons. The correct expression is given in Eqs. (10) and (11) of Dixit and McKoy,[19] and we refer the reader to this paper for further discussions on the calculation of the radial terms. However, this oversight in Eqs. (A24a) of KSZ is of no significance when trying to determine rotational populations and polarizations.

Figure 10 depicts $I(J_i,M_i)$ vs M_i for $J=10$ for the five rotational branches, and for $u=-1$, 0, and $+1$. Looking at the plot for the O branch [see Fig. 10(e)], for linearly polarized light ($u=0$), the curve is symmetric about $M_i=0$ because $\Delta M=M_f-M_i=0$, and $I(J_i,M_i)$ is zero for $|M_i|>7$ because these transitions would result in forbidden states: $M_f>J_f$. For left circularly polarized light ($u=-1$), $I(J_i,M_i)$ is zero for $M_i<-5$ and $I_{\max}$ occurs at $M_i=9$ because left circularly polarized light causes $\Delta M=-2$. Similarly for right circularly polarized light ($u=+1$), because $\Delta M=+2$, $I(J_i,M_i)$ is zero for $M_i>5$ and $I_{\max}$ is located at $M_i=-9$.

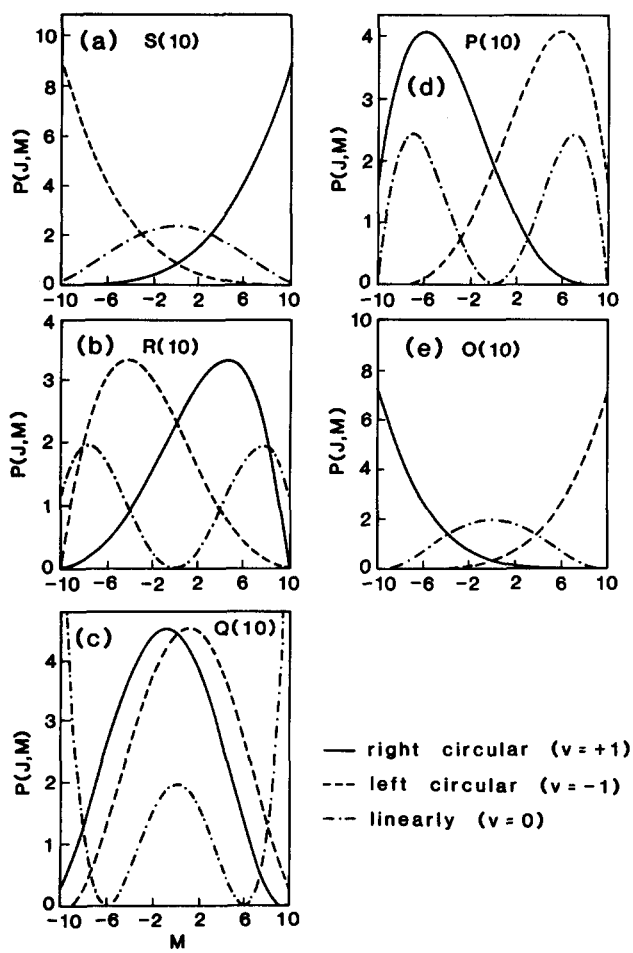

FIG. 10. Excitation probability $P(J,M)$ vs magnetic quantum number M for right circularly polarized light, linearly polarized light, and left circularly polarized light propagating along the z axis for $J_i=10$ in the N_2 $a\,^1\Pi_g$–$X\,^1\Sigma_g^+$ two-photon transition.

For the S branch the exact opposite trends are seen [see Fig. 10(a)]: for left circularly polarized light ($u=-1$), $I_{\max}$ occurs at $M_i=-9$, and for right circularly polarized light ($u=+1$), $I_{\max}$ occurs at $M_i=9$. Hence, if we observe an enhancement of the S branch relative to the O branch for a sample irradiated by circularly polarized light, the molecules are rotating in the same direction as the photons. To figure out which direction the molecules are rotating, one must determine the direction of rotation of the light. This may be done using a single Fresnel rhomb.[20]

Hecht and Zajac[20] define right circularly polarized light as that which has a clockwise rotation when the observer is looking down the laser propagation axis, looking in the same direction as the laser beam is propagating. However, we associate positive M_i states with clockwise rotation for an observed looking down the $z_{\rm lab}$ axis. For case I geometry, the light is propagating along the $-z$ axis and the $P_{0+}^{\{1\}}$ line strength for the S branch is positive for $\beta=-45°$; hence since $A_{0+}^{\{1\}}=\langle|J_z/\mathbf{J}|\rangle$, $\beta=-45°$ must be associated with right-handed circularly polarized light. For case II, we are propagating along the $-x$ direction so once again $\beta=-45°$ corresponds to right circularly polarized light. For case III, the light is propagating along the $+y$ axis so $\beta=+45°$ corresponds to right circularly polarized light. Remember, the sense of rotation of the light is for an observer looking down the laser propagation axis while the direction of rotation for J_x,J_y, and J_z are referenced to the lab fixed coordinate system.

From Figs. 10(b) and 10(d), we see that for the $\Delta J=\pm1$ branches, $I_{\max}$ does not occur at $M_i=\pm J_i$. Hence, we would expect that these branches would have smaller line strengths for the dipole moments, and this is seen in Figs. 3–7. Figure 10(c) shows that the Q branch is almost insensitive to differences between left and right circularly polarized light. Hence, we expect that the orientation line strength for the Q branch would be very small, and this is seen in Figs. 3–7.

ACKNOWLEDGMENTS

We would like to thank R. B. Bernstein, and A. J. McCaffery for many useful discussions. We are greatly indebted to J. R. Waldeck for proofreading this manuscript. The computations were performed at the Stanford Cell Biology Computer Center under N.S.F. DMB 84-00396 with the assistance of D. E. Austin and B. Hurja. We would also like to acknowledge the assistance of J. Choi and D. A. V. Kliner in preparing the figures. This project was supported by the Office of Naval Research under N00014-87-K-0265.

APPENDIX

1. Derivation of the geometric factor $\epsilon_{q+}^{\{k\}}(k_d,k_a;\Omega)$

We can use all the derivations given by KSZ except Eqs. (A31)–(A45) because these equations are applicable only

for linearly polarized light. Our starting equation is Eq. (A30) of KSZ:

$$\epsilon_q^{(k)}(k_d,k_a;\Omega_{\rm det}) = (-1)^{k_a-k_d-q}(2k+1)^{1/2} \times \sum_m \begin{pmatrix} k_d & k_a & K \\ m & q-m & -q \end{pmatrix} E^{k_d}_m E^{k_a}_{q-m}, \quad \text{(A1)}$$

where $E^k_q = [e^{(1)^*} \otimes e^{(1)}]^k_q$. In our previous paper we were able to break up these remaining cross products and separate the geometric factor into some coupling constants multiplied by a spherical harmonic that depended on k and q but not on k_a and k_d. In the general case, this is no longer possible since the electric field vector of the light is now a complex quantity and requires at least three variables to specify its state: two angles which describe the location of the plane of polarization and another variable which describes its ellipticity. The spherical harmonics are functions of only two variables; hence, elliptically polarized light cannot be described by a spherical harmonic function alone.

The best way to calculate the cross products in Eq. (A1) is by expanding them into the cartesian components of the electric field vectors. From Table VI of KSZ and Eq. (A29) of KSZ: $e^1_{+1} = (-1/\sqrt{2})(e_x + ie_y)$; $e^1_0 = e_z$; $e^1_{-1} = (1/\sqrt{2})(e_x - ie_y)$, and

$$[e^{*(1)} \otimes e^{(1)}]^k_q = (-1)^{k_2-k_1-q}(2k+1)^{1/2} \times \sum_m \begin{pmatrix} k_1 & k_2 & k \\ m & q-m & -q \end{pmatrix} e^{*k_1}_m e^{k_2}_{q-m}. \quad \text{(A2)}$$

The specific cross products for $k = 0,1,2$ are given in Table X. We note that to calculate the moments of e^*, you merely replace e_x, e_y, and e_z by their complex conjugates in the equations for the e^k_q but leave the signs on "i" untouched. For example, $e^{*1}_{+1} = (e^*)^1_{+1} = (-1/\sqrt{2})(e^*_x + ie^*_y)$.

To transform Eq. (A1) to the detector reference frame we employ Eq. (4.8) of Brink and Satchler.[21] We follow the GZ and KSZ conventions [see Eq. (A3) of GZ and (A43) of KSZ] of designating the Euler angles (ϕ,θ,χ) as rotating the lab into the detector frame. Since the photons are identical, we can rotate the geometric factor directly instead of rotating the E^k_q individually as was done by GZ; this direct rotation greatly reduces the computational complexity:

$$\epsilon_q^{(k)}(k_d,k_a;\Omega_{\rm lab}) = \sum_{q'} D^{k*}_{q,q'}(\phi,\theta,\chi)\epsilon^{(k)}_{q'}(k_d,k_a;\Omega_{\rm det}). \quad \text{(A3)}$$

TABLE X. Cross products of the electric field vectors expressed in Cartesian components. Note $e^* \cdot e = 1$.

$[e^{*1} \otimes e^1]^0_0 = -1/\sqrt{3}$
$[e^{*1} \otimes e^1]^1_0 = (i/\sqrt{2})(e^*_x e_y - e^*_y e_x)$
$[e^{*1} \otimes e^1]^1_{\pm 1} = (1/2)[(e^*_z e_x - e^*_x e_z) \pm i(e^*_z e_y - e^*_y e_z)]$
$[e^{*1} \otimes e^1]^2_0 = (1/\sqrt{6})(3e^*_z e_z - 1)$
$[e^{*1} \otimes e^1]^2_{\pm 1} = (\mp 1/2)[(e^*_z e_x + e^*_x e_z) \pm i(e^*_z e_y + e^*_y e_z)]$
$[e^{*1} \otimes e^1]^2_{\pm 1} = (1/2)[(e^*_x e_x - e^*_y e_y) \pm i(e^*_x e_y + e^*_y e_x)]$

We convert the complex conjugate rotation matrix element into a reduced rotation matrix element using Eqs. (2.15) and (2.17) of Brink and Satchler[21]:

$$\epsilon_q^{(k)}(k_d,k_a;\Omega_{\rm lab}) = \sum_{q'} e^{iq'\chi} d^k_{q',q}(-\theta) e^{iq\phi} \epsilon^{(k)}_q(k_d,k_a;\Omega_{\rm det}). \quad \text{(A4)}$$

Substituting Eq. (A1) into Eq. (A4), we derive the general equation for the geometric factor:

$$\epsilon_q^{(k)}(k_d,k_a;\Omega_{\rm lab}) = \sum_{q'} e^{iq'\chi} d^k_{q',q}(-\theta) e^{iq\phi} \times \sum_m (-1)^{k_a-k_d-q'}(2k+1)^{1/2} \times \begin{pmatrix} k_d & k_a & k \\ m & q'-m & -q' \end{pmatrix} E^{k_d}_m E^{k_a}_{q'-m}. \quad \text{(A5)}$$

Finally, we must convert to the Hertel–Stoll[15] normalization because the geometric factor will, in general, be complex when detecting orientation moments with elliptically polarized light. In the Hertel–Stoll normalization the geometric factor is always real. Another benefit of this renormalization is a reduction in the number of detectable moments. For example, if J_x has a nonzero expectation value, this would normally result in two nonzero dipole moments, $A^{(1)}_{+1}$ and $A^{(1)}_{-1}$, but in the Hertel–Stoll[15] normalization it would result in only one nonzero dipole moment, $A^{\{1\}}_{1+}$ (see Table VI). We can use Eqs. (A49a) – (A49c) of KSZ along with Table V of this paper to arrive at a more straightforward transformation to the Hertel–Stoll[15] normalization:

$$T^{\{k\}}_{q+} = (-1)^q(2-\delta_{q,0})^{1/2}{\rm Re}(T^{(k)}_q), \quad q \geqslant 0 \quad \text{(A6)}$$

and

$$T^{\{k\}}_{q-} = (-1)^q(1-\delta_{q,0})(2)^{1/2}{\rm Im}(T^{(k)}_q), \quad q \geqslant 0. \quad \text{(A7)}$$

We note that Eqs. (A6) and (A7) as well as Eqs. (A49a)–(A49c) of KSZ and Eqs. (13) and (14) of Ref. 15 only produce real tensor operators if the original standard operators $T^{(k)}_{\pm q}$ are of the form $T^{(k)}_{\pm q={\rm even}} = {\rm Re} \pm i\,{\rm Im}$ and $T^{(k)}_{\pm q={\rm odd}} = \pm {\rm Re} + i\,{\rm Im}$ where "Re" is the real part of the operator and "Im" is the imaginary part of the operator. These conditions are fulfilled by the geometric factor. Hence

$$\epsilon^{\{k\}}_{q+}(k_d,k_a;\Omega_{\rm lab}) = (-1)^q(2-\delta_{q,0})^{1/2}{\rm Re}[\epsilon^{(k)}_q(k_d,k_a;\Omega_{\rm lab})], \quad q \geqslant 0 \quad \text{(A8)}$$

and

$$\epsilon^{\{k\}}_{q-}(k_d,k_a;\Omega_{\rm lab}) = (-1)^q(1-\delta_{q,0})(2)^{1/2}{\rm Im}[\epsilon^{(k)}_q(k_d,k_a;\Omega_{\rm lab})], \quad q \geqslant 0. \quad \text{(A9)}$$

We note that Eqs. (A6) and (A7) have been used along with the equations given in the footnotes in Table V to generate the $J^{\{k\}}_{q\pm}$ and $A^{\{k\}}_{q\pm}$. The conditions for the use of Eqs. (A6) and (A7) are only satisfied if the $J^{(k)}_{\pm q}$ are calculated in the manner of the CMH (see discussion at the bottom of Table V).

2. Determination of the electric field vector Cartesian components and the Euler angles for the three geometries

a. General geometry and case I geometry

Let us assume that we start with linearly polarized light whose polarization vector $\hat{\mathbf{B}}$ can be varied via a half-wave plate or an equivalent device (see Fig. 1). We designate the detector frame as follows: the light is propagating along the $-z_d$ axis, x_d lies along the major axis of the variable phase shift plate, and y_d lies along the minor axis of the variable phase shift plate. Due to the anisotropy in the index of refraction, the wave plate induces a phase shift δ for the component of the photons' electric field vector along the y_d axis. Thus according to Fano,[16] we can model the effect of the variable phase shift plate upon the photons' electric field vector as follows:

$$\hat{\mathbf{e}}_{\text{before}}(\text{linear}) = \exp(i\omega t)(\cos\beta\hat{\mathbf{x}}_d + \sin\beta\hat{\mathbf{y}}_d), \tag{A10}$$

$$\hat{\mathbf{e}}_{\text{after}}(\text{elliptical}) = \exp(i\omega t)(\cos\beta\hat{\mathbf{x}}_d + e^{i\delta}\sin\beta\hat{\mathbf{y}}_d). \tag{A11}$$

There is one special case: a quarter-wave plate, ($\delta = \pi/2$):

$$\hat{\mathbf{e}}(1/4\text{-wave plate}) = \exp(i\omega t)(\cos\beta\hat{\mathbf{x}}_d + i\sin\beta\hat{\mathbf{y}}_d). \tag{A12}$$

Hence, for case I geometry $e_x = \cos\beta$, $e_y = \exp(i\delta)\sin\beta$, $e_z = 0$.

These equations are used to evaluate the cross products in Table X and to produce the E_q^k for case I geometry in Table III. We can then use Eq. (A5) and a set of Euler angles to relate the detection frame to any lab frame. However, if we restrict ourselves to case I geometry, we can greatly simplify Eq. (A5) since case I geometry fixes two of the Euler angles. In case I geometry the laser is propagating along the $-z$ direction and the x_d–y_d plane is parallel to the x–y plane. Consequently, two of the Euler angles are zero: $\chi = 0$ and $\theta = 0$. In Fig. 2(a) we have defined Δ to be a clockwise rotation about z while the Euler angle ϕ causes a counterclockwise rotation about z. Consequently, we define $\phi = -\Delta$. Substituting these Euler angles into Eq. (A5), we get:

$$\epsilon_q^{(k)}(k_d,k_a;\Omega_{\text{lab}}) = [\cos(q\Delta) - i\sin(q\Delta)](-1)^{k_a-k_d-q}(2k+1)^{1/2} \times\sum_m \begin{bmatrix} k_d & k_a & k \\ m & q-m & -q \end{bmatrix} E^{k_d}_m E^{k_a}_{q-m}. \tag{A13}$$

b. Case II geometry

We can directly use the general equation for the geometric factor and the E_q^k for case I geometry along with the Euler angles $(0,\pi/2,\pi-\Delta)$ to evaluate the case II geometric factor. Alternately, we can directly label the major axis of the wave plate as z_d and the minor axis as $-y_d$ and calculate a new set of E_q^k specific to case II geometry. For case II geometry, $e_z = \cos\beta$, $e_y = -\exp(i\delta)\sin\beta$, and $e_x = 0$. If the major axis of the wave plate is kept fixed along z, ($\Delta = 0$), then all the Euler angles are zero. In general, we must allow the wave plate to rotate in the y–z plane. Designating Δ as a clockwise rotation, the Euler angles are $(\phi = \pi/2, \theta = \Delta, \chi = -\pi/2)$. Substituting the Euler angles into Eq. (A9) and E_q^k for case II geometry (see Table III), we get a simplified equation:

$$\epsilon_q^{(k)}(k_d,k_a;\Omega_{\text{lab}}) = [\cos(q\pi/2) + i\sin(q\pi/2)] \times\sum_{q'} d^k_{q',q}(-\Delta)[\cos(q'\pi/2) - i\sin(q'\pi/2)] \times\sum_m (-1)^{k_a-k_d-q'}(2k+1)^{1/2} \times\begin{pmatrix} k_d & k_a & k \\ m & q'-m & -q' \end{pmatrix} E^{k_d}_m E^{k_a}_{q'-m}. \tag{A14}$$

c. Case III geometry

We can directly use the general equation for the geometric factor and the E_q^k for case I geometry along with the Euler angles $(-\pi/2,\pi/2,\pi-\Delta)$ to evaluate the case III geometry factor. Alternately, we can directly label the major axis of the wave plate as z_d and the minor axis as $-x_d$ and calculate a new set of E_q^k specific to case III geometry. For case III geometry, $e_z = \cos\beta$, $e_x = -\exp(i\delta)\sin\beta$, and $e_y = 0$. We allow the major axis of the wave plate to rotate in the z–x plate. Since the Euler angle θ describes a clockwise rotation about y and Δ is also a clockwise rotation about y, we can set the Eulger angles equal to $(0,\Delta,0)$. Using these Euler angles along with the E_q^k for case III geometry, we can simplify Eq. (A5):

$$\epsilon_q^{(k)}(k_d,k_a;\Omega_{\text{lab}}) = \sum_{q'} d^k_{q',q}(-\Delta)\sum_m (-1)^{k_a-k_d-q'}(2k+1)^{1/2} \times\begin{pmatrix} k_d & k_a & k \\ m & q'-m & -q' \end{pmatrix} E^{k_d}_m E^{k_a}_{q'-m}. \tag{A15}$$

3. Geometric factors for linearly polarized light

We will derive simplified equations for the geometric factors for the case that the light is linearly polarized. These equations are free of reduced rotation matrix elements and are free of summations (except for case I) and, hence, are quite facile to calculate. The equation for case III was given in our previous paper and our ability to regenerate it shows the link between the results in this paper with the results in KSZ. The equations for cases I and II are new. All three equations can be used when trying to determine the alignment moments [see Eqs. (36) and (38)] and are most useful in Appendix Sec. 4 when we calculate the expansion coefficients for the apparent moments [see Eq. (36) and Table IX]. We will derive the equations for linearly polarized light directly from the equations in this paper rather than using KSZ, but we will compare the results. We start with case III since all other geometries can be related to this most simple geometry via Euler rotations.

a. Case III geometry

For linearly polarized light, $\beta = 0°$, the only nonzero E^k_q are those with $q = 0$: $E^0_0 = -1/\sqrt{6}$ and $E^2_0 = 2/\sqrt{6}$. This implies that in Eq. (A15) $m = 0$, $q' - m = 0$, and hence $q' = 0$. This removes both summations in Eq. (A15). Hence:

$$\epsilon^{(k)}_q(k_d,k_a;\beta=0)(\text{lab}) = d^k_{0,q}(\Delta)(2k+1)^{1/2} \times \begin{pmatrix} k_d & k_a & k \\ 0 & 0 & 0 \end{pmatrix} E^{k_d}_0 E^{k_a}_0. \tag{A16}$$

Note: we were able to remove the phase factor from Eq. (A15) since k_d and k_a are even and since $d^k_{0,q}(-\Delta) = (-1)^q d^k_{0,q}(\Delta)$. Next we make two substitutions:

$$E^k_0 = (2k+1)^{1/2} \begin{pmatrix} 1 & 1 & k \\ 0 & 0 & 0 \end{pmatrix} \text{ for } k = 0,2 \text{ only} \tag{A17}$$

and

$$d^k_{0,q}(\Delta) = [4\pi/(2k+1)]^{1/2} Y^k_q(\Delta,0). \tag{A18}$$

Equation (A17) was derived by induction. Substituting Eqs. (A17) and (A18) into Eq. (A16), we find

$$\epsilon^{(k)}_q(k_d,k_a;\beta=0)(\text{case III}) = [4\pi(2k_a+1)(2k_d+1)]^{1/2} \times \begin{pmatrix} 1 & 1 & k_d \\ 0 & 0 & 0 \end{pmatrix} \begin{pmatrix} 1 & 1 & k_a \\ 0 & 0 & 0 \end{pmatrix} \begin{pmatrix} k_d & k_a & k \\ 0 & 0 & 0 \end{pmatrix} \times Y^k_q(\Delta,0). \tag{A19}$$

This equations is identical to the one for the geometric factor in Table IV of KSZ.

b. Case II geometry

To rotate case II geometry into case III geometry, we perform a Euler rotation of $\chi = \pi/2$ about the z axis. Using an equation analogous to Eq. (A4), we derive

$$\epsilon^{(k)}_q(k_d,k_a,\beta=0)(\text{case II}) = e^{iq\pi/2}\epsilon^{(k)}_q(k_d,k_a,\beta=0)(\text{case III}). \tag{A20}$$

Substituting Eq. (A19) into Eq. (A20),

$$\epsilon^{(k)}_q(k_d,k_a;\beta=0)(\text{case II}) = [4\pi(2k_a+1)(2k_d+1)]^{1/2} \times \begin{pmatrix} 1 & 1 & k_d \\ 0 & 0 & 0 \end{pmatrix} \begin{pmatrix} 1 & 1 & k_a \\ 0 & 0 & 0 \end{pmatrix} \begin{pmatrix} k_d & k_a & k \\ 0 & 0 & 0 \end{pmatrix} \times Y^k_q(\Delta,\pi/2). \tag{A21}$$

c. Case I geometry

For linearly polarized light, $\beta = 0$, and case I geometry, there are, unfortunately, four nonzero E^k_q: $E^0_0 = -1/\sqrt{3}$, $E^2_{\pm 2} = 1/2$, and $E^2_0 = -1/\sqrt{6}$. Hence, we cannot remove the summation in the case I equation for the geometric factor [see Eq. (A13)]. However, we can segregate the portion of the geometric factor which depends on Δ from the part of the geometric factor which depends on k_a and k_d. Substituting the identity $Y^k_q(\pi/2,-\Delta)/Y^k_q(\pi/2,0) = [\cos(q\Delta) - i\sin(q\Delta)]$ into Eq. (A13), we find

$$\epsilon^{(k)}_q(k_d,k_a;\beta=0)(\text{case I}) = (-1)^{k_a-k_d-q}(2k+1)^{1/2}[Y^k_q(\pi/2,-\Delta)/Y^k_q(\pi/2,0)] \sum_{m=0,\pm 2} \begin{pmatrix} k_d & k_a & k \\ m & q-m & -q \end{pmatrix} E^{k_d}_m E^{k_a}_{q-m}. \tag{A22}$$

This may not seem so simple, but since the only part of the geometric factor which depends on the polarization is now outside of the summation, it will be very easy to calculate the expansion coefficients for the apparent moments [see Eq. (A31)].

4. The apparent moments

a. General

As previously stated, when detecting the alignment with linearly polarized light propagating along a fixed direction, the line strengths do not vary independently with Δ. In addition, when detecting orientation with elliptically polarized light with the major axis of ellipticity fixed in space (constant Δ) and the light propagating along a fixed direction, the line strengths do not vary independently with β. For example, as seen in Eq. (A13), for case I geometry, the geometric factor's variation with Δ only depends upon q and is independent of k. In order to analyze data taken from one or two rotational branches with linearly polarized light, we need to reformulate Eq. (1) so that we are only using line strengths which are independent over the plane of space in which we are varying the light's polarization vector.

For each geometry there will be only five $P^{\{k\}}_{q\pm}$ which vary independently with Δ and seven $P^{\{k\}}_{q\pm}$ which vary independently with β; these will be denoted as the $P^{\{k\}}_{q\pm}(\text{ind})$ the remaining line strengths are designated as $P^{\{k\}}_{q\pm}(\text{dep})$. For variation of Δ, the reason that there are only five independent line strengths can be seen in Eq. (A22). For case I geometry, the dependence of $P^{\{k\}}_{\pm q}$ on Δ is only a function of q, and there are only five allowed values of q, $q = 0, \pm 2, \pm 4$. In addition, for any other fixed geometry there are only five $P^{\{k\}}_{\pm q}(\text{ind})$ for variation of Δ because rotating the coordinate frame does not change the dimensionality of the coordinate space. For either orientation or alignment experiments, the $P^{\{k\}}_{q\pm}(\text{dep})$ must be expressed as functions of these independent $P^{\{k\}}_{q\pm}(\text{ind})$ in order to determine which $A^{\{k\}}_{q\pm}$ we are measuring:

$$P^{\{k\}}_{q\pm}(J_i,J_f,\beta,\Delta)(\text{dep}) = \sum_{k',q'} c(k,q,k',q')R(k,q,k',q',J_i,J_f) \times P^{\{k'\}}_{q'\pm}(J_i,J_f,\beta,\Delta)(\text{ind}), \tag{A23}$$

where k' and q' are the ranks and components of the five/seven independent line strengths. The specific k' and q' of the independent line strengths depend upon the detection geometry.

For variation of β, the choice of $P^{\{k\}}_{q\pm}$ (ind) is not unique except that all the moments with odd k must be included in the set of independent moments. For orientation measurements, the portion of $P^{\{k\}}_{q\pm}$ which depends on β cannot be separated from the dependence on k_a and k_d. Consequently, we cannot independently determine the two expansion coefficients in Eq. (A23) but only their product $c(k,q,k',q',J_i,J_f) = c(k,q,k',q')\,R(k,q,k',q',J_i,J_f)$. For orientation measurements, the $c(k,q,k',q',J_i,J_f)$ are determined by numerically solving Eq. (A23).

For variation of Δ with $\beta = 0°$, the five independent line strengths are orthogonal in the plane of the light's polarization vector if that plane is perpendicular to the x, y, or z axes of the laboratory frame. To evaluate the constants in Eq. (A23), we multiply both sides of the equation by $P^{\{k'\}}_{q'\pm}$ and integrate over the plane of space in which the polarization vector of the light rotates:

$$R(k,q,k'q',J_i,J_f)c(k,q,k',q') = \frac{\int_{\theta=0}^{\theta=\pi}\int_{\phi=0}^{\phi=2\pi} P^{\{k'\}}_{q'\pm}(J_i,J_f,\beta=0,\Delta)(\text{ind})P^{\{k\}}_{q\pm}(J_i,J_f,\beta=0,\Delta)(\text{dep})\sin\theta\,d\phi\,d\theta}{\int_{\theta=0}^{\theta=\pi}\int_{\phi=0}^{\phi=2\pi} P^{\{k'\}}_{q'\pm}(J_i,J_f,\beta=0,\Delta)(\text{ind})P^{\{k'\}}_{q'\pm}(J_i,J_f,\beta=0,\Delta)(\text{ind})\sin\theta\,d\phi\,d\theta}. \tag{A24}$$

In Eq. (A24), θ and ϕ refer to the polar angles the electric field vector makes in the x–z and x–y planes. Specifically, we employ the same definition as that used when defining the spherical harmonics $Y^k_q(\theta,\phi)$. Later we will explicitly give a relationship between Δ and these polar angles for our three special geometries. Note, the integration limits in Eq. (A24) may depend on the specific experimental geometry.

The expansion coefficients in Eqs. (A23) and (A24) have been broken into two parts: $c(k,q,k',q')$ is the projection of the part of the $P^{\{k\}}_{q\pm}$ (dep) which depends on Δ onto the part of $P^{\{k'\}}_{q'\pm}$ (ind) which depends on Δ; $R(k,q,k',q',J_i,J_f)$ is the ratio of the part of the $P^{\{k\}}_{q\pm}$ (dep) which is independent of Δ to the part of $P^{\{k'\}}_{q'\pm}$ (ind) which is independent of Δ. It is the portion of the fraction in Eq. (A24) which can be brought outside the integrals.

All of $P^{\{k\}}_{q\pm}$ except $\epsilon^{\{k\}}_{q\pm}$ is independent of Δ and can be brought outside the integrals in Eq. (A24). In addition, part of the geometry factor is independent of Δ. Comparing Eqs. (A19), (A21), and (A22), we see that for case III geometry, the geometry factor is most easily separated into two parts: the first part is independent of Δ, and the second part depends on Δ. To separate the general geometric factor into two parts, let (ϕ',θ',χ') be the Euler angles which rotate case III geometry into any given geometry:

$$\begin{aligned}\epsilon^{\{k\}}_{q\pm}(J_i,J_f,\beta=0,\Delta)(\text{lab}) &= \sum_{q'\pm} D^{\{k\}*}_{q'\pm,q\pm}(\phi',\theta',\chi')\epsilon^{\{k\}}_{q'\pm}(J_i,J_f,\beta=0,\Delta)(\text{case III})\\ &= [4\pi(2k_a+1)(2k_d+1)]^{1/2}\begin{pmatrix}1 & 1 & k_d\\ 0 & 0 & 0\end{pmatrix}\begin{pmatrix}1 & 1 & k_a\\ 0 & 0 & 0\end{pmatrix}\begin{pmatrix}k_d & k_a & k\\ 0 & 0 & 0\end{pmatrix}\\ &\times\sum_{q'\pm} D^{\{k\}*}_{q\pm,q'\pm}(\phi',\theta',\chi')Y^{\{k\}}_{q'\pm}(\Delta,0).\end{aligned} \tag{A25}$$

In Eqs. (A25) we employed the real rotation matrices, $D^{\{k\}}_{q\pm,q'\pm}$, which are defined in Eq. (15) of Ref. 15. If one wishes to avoid using the real rotation matrices, the complex $\epsilon^{(k)}_q$ can be rotated and then converted to the real $\epsilon^{\{k\}}_{q\pm}$. The $Y^{\{k\}}_{q\pm}$ are the spherical harmonic function in the Hertel–Stoll notation and can be calculated using Eqs. (A6) and (A7) and a table of spherical harmonics, such as that given in Mathews.[22]

Equation (A25) neatly splits the geometric factor into two parts. The first part consists of the square roots of numbers times the products of 3 — J symbols; it is independent of the system geometry. We name the second part $G(k,q,\phi',\theta',\chi',\Delta)$; it represents the portion of the geometric factor which depends on the direction of polarization of the light:

$$G(k,q,\phi',\theta',\chi',\Delta) = \sum_{q'\pm} D^{\{k\}*}_{q\pm,q'\pm}(\phi',\theta',\chi')Y^{\{k\}}_{q'\pm}(\Delta,0). \tag{A26}$$

Hence, $P^{\{k\}}_{q\pm}(J_i,J_f,\beta=0,\Delta)/G(k,q,\phi',\theta',\chi',\Delta)$ is the portion of the geometric factor which is independent of the Euler angles and Δ. To calculate $R(k,q,k',q',J_i,J_f)$, the ratio of the part of the $P^{\{k\}}_{q\pm}$ (dep) which is independent of Δ to the part of $P^{\{k'\}}_{q'\pm}$ (ind) which is independent of Δ, we compare $P^{\{k\}}_{q\pm}/G$ with $P^{\{k'\}}_{q'\pm}/G$:

$$R(k,q,k',q',J_i,J_f) = \frac{P^{\{k\}}_{q\pm}(J_i,J_f,\beta=0,\Delta)/G(k,q,\phi',\theta',\chi',\Delta)}{P^{\{k'\}}_{q'\pm}(J_i,J_f,\beta=0,\Delta)(\text{dep})/G(k',q',\phi',\theta',\chi',\Delta)}. \tag{A27}$$

To calculate $c(k,q,k',q')$ we substitute Eqs. (A25) and (A26) into Eq. (A24) and then divide by Eq. (A27). The result, $c(k,q,k',q')$, is the projection of $G(k,q)$ onto $G(k',q')$ over the plane of polarization:

$$c(k,q,k',q') = \frac{\int_{\theta=0}^{\theta=\pi}\int_{\phi=0}^{\phi=2\pi} G(k,q,\phi',\theta',\chi',\Delta)G(k',q',\phi',\theta',\chi',\Delta)\sin\theta\,d\phi\,d\theta}{\int_{\theta=0}^{\theta=\pi}\int_{\phi=0}^{\phi=2\pi} G(k',q',\phi',\theta',\chi',\Delta)G(k',q',\phi',\theta',\chi',\Delta)\sin\theta\,d\phi\,d\theta}. \tag{A28}$$

Note that k' and q' are the indices for the independent line strengths while k and q are the indices for the dependent line strengths. The $G(k,q,\phi,\theta,\chi,\Delta)$ have simple forms for the three special geometries:

$$G(k,q,\Delta)(\text{case I}) = Y_{q\pm}^{\{k\}}(\pi/2,-\Delta), \tag{A29}$$

$$G(k,q,\Delta)(\text{case II}) = Y_{q\pm}^{\{k\}}(\Delta,\pi/2), \tag{A30}$$

$$G(k,q,\Delta)(\text{case III}) = Y_{q\pm}^{\{k\}}(\Delta,0). \tag{A31}$$

To perform the integration in Eq. (A28), we substitute the appropriate equation for $G(k,q,\Delta)$ and replace Δ by ϕ(case I) or θ(cases II and III).

Equations (A23)–(A28) and (A29)–(A31) were used to prepare Table IX and were checked numerically by doing a linearly least-squares fit of the $P_{q\pm}^{\{k\}}$(dep) to the $P_{q\pm}^{\{k\}}$(ind) for each geometry.

Once we have derived the coefficients in Eq. (A23), we can revise Eq. (2) so that we can express the intensity as a function of the apparent moments. Substituting Eq. (A23) for each $P_{q\pm}^{\{k\}}$(dep) and grouping together all the coefficients for each $P_{q\pm}^{\{k\}}$(ind) and renaming these coefficients as the $A_{q\pm}^{\{k\}}$(app):

$$I = C(\text{det})n(J_i) \times \sum_{k,q} [P_{q\pm}^{\{k\}}(J_i,\Lambda_i,J_f,\Lambda_f;\Omega)(\text{ind})A_{q\pm}^{\{k\}}(\text{app}) + P_{q-}^{\{k\}}(J_i,\Lambda_i,J_f,\Lambda_f;\Omega)(\text{ind})A_{q-}^{\{k\}}(\text{app})], \tag{A32}$$

where

$$A_{q\pm}^{\{k\}}(J_i,J_f,\beta=0,\Delta)(\text{app}) = \sum_{k',q'} c(k',q',k,q)R(k',q',k,q,J_i,J_f) \times A_{q'\pm}^{\{k'\}}(J_i,J_f,\beta=0,\Delta), \tag{A33}$$

and where the k and q in Eq. (A32) are restricted to the ranks and components for the five $P_{q\pm}^{\{k\}}$(ind), but the k' and q' in Eq. (A33) are completely general. Note that since $R(k',q',k,q,J_i,J_f)$ are explicitly functions of J_f, the $A_{q\pm}^{\{k\}}$(app) are different for each rotational branch. This means that if two rotational branches are being probed, separate $A_{q\pm}^{\{k\}}$(app) should be calculated for each branch. Afterwards the two sets of apparent moments can be compared and inferences can be drawn about the real $A_{q\pm}^{\{k\}}$.

[1] A. C. Kummel, G. O. Sitz, and R. N. Zare, J. Chem. Phys. **85**, 6875 (1986).

[2] S. R. Jeyes, A. J. McCaffery, M. D. Rowe, and H. Kato, Chem. Phys. Lett. **48**, 91 (1977); M. D. Rowe and A. J. McCaffery, Chem. Phys. **34**, 81 (1978); M. D. Rowe and A. J. McCaffery, *ibid.* **43**, 35 (1979).

[3] J. Macek and D. Burns in *Topics in Current Physics, Beam Foil Spectroscopy*, edited by S. Bashkin (Springer, Berlin, 1976), Vol. 1; H. J. Andra, in *Progress in Atomic Spectroscopy*, edited by W. Hanle and H. Kleinpoppen (Plenum, New York, 1979), Part B.

[4] A. J. Bain, A. J. McCaffery, M. J. Proctor, and B. J. Whitaker, Chem. Phys. Lett. **110**, 663 (1984); A. J. Bain and A. J. McCaffery, J. Chem. Phys. **83**, 2627, 2632 (1985).

[5] A. J. Bain and A. J. McCaffery, J. Chem. Phys. **83**, 2641 (1985).

[6] D. A. Case, G. M. McClelland, and D. R. Herschbach, Mol. Phys. **35**, 541 (1978).

[7] P. R. Brooks and E. M. Jones, J. Chem. Phys. **45**, 3449 (1966); P. R. Brooks, *ibid.* **50**, 5031 (1969); Faraday Discuss. Chem. Soc. **55**, 299 (1973); Science **193**, 11 (1976); G. Marcelin and P. R. Brooks, J. Am. Chem. Soc. **97**, 1710 (1975); P. R. Brooks, J. S. McKillop, and H. G. Pippin, Chem. Phys. Lett. **66**, 144 (1979); S. L. Anderson, P. R. Brooks, J. D. Fite, and O. Van Hguyen, J. Chem. Phys. **72**, 6521 (1980); H. S. Carmen, P. W. Harland, and P. R. Brooks, J. Phys. Chem. **90**, 944 (1986).

[8] H. G. Bennewitz, K. H. Kramer, W. Paul, and J. P. Toennies, Z. Phys. **177**, 84 (1964); J. P. Toennies, *ibid.* **182**, 257 (1965); H. G. Bennewitz, R. Gengenbach, R. Haerten, and G. Muller, *ibid.* **266**, 279 (1969); U. Borkenhagen, H. Malthan, and J. P. Toennies, Chem. Phys. Lett. **41**, 222 (1976).

[9] R. J. Beuhler, Jr. and R. B. Bernstein, J. Chem. Phys. **51**, 5306 (1969); D. H. Parker, K. K. Chakravorty, and R. B. Bernstein, *ibid.* **85**, 466 (1981); **86**, 113 (1982).

[10] D. van den Ende and S. Stolte, Chem. Phys. **89**, 121 (1984); Chem. Phys. Lett. **76**, 13 (1980); D. van den Ende, S. Stolte, J. B. Cross, G. H. Kwei, and J. J. Valentini, J. Chem. Phys. **77**, 2206 (1982); D. H. Jalink, F. Harren, D. van den Ende, and S. Stolte, Chem. Phys. **108**, 391 (1986); H. Jalink, D. H. Parker, K. H. Meiwes-Broer, and S. Stolte, J. Phys. Chem. **90**, 552 (1986); H. Jalink, D. H. Parker, and S. Stolte, *ibid.* **85**, 5372 (1986).

[11] H. Moerkerken, M. Prior, and J. Reuss, Physica **50**, 499 (1970); S. Stolte, J. Reuss, and H. L. Schwartz, *ibid.* **57**, 254 (1972); **66**, 211 (1973); H. L. Schwartz, S. Stolte, and J. Reuss, Chem. Phys. **2**, 1 (1973); S. Stolte, J. Reuss, and H. L. Schwartz, Physica **66**, 211 (1973); H. Moerkerken, L. Zandee, and J. Reuss, Chem. Phys. **87**, 87 (1975); H. Thuis, S. Stolte, and J. Reuss, *ibid.* **43**, 351 (1979).

[12] S. R. Gandhi, T. J. Curtiss, Q. X. Xu, S. E. Choi, and R. B. Bernstein, Chem. Phys. Lett. **132**, 6 (1986); S. R. Gandhi, Q. X. Xu, T. J. Curtiss, and R. B. Bernstein, J. Phys. Chem. **91**, 5437 (1987); S. R. Gandhi, T. J. Curtiss, and R. B. Bernstein, Phys. Rev. Lett. **59**, 2951 (1987).

[13] S. R. Jeyes, A. J. McCaffery, and M. D. Rowe, Mol. Phys. **36**, 845, 1865 (1978).

[14] G. O. Sitz, A. C. Kummel, and R. N. Zare, J. Chem. Phys. **87**, 3247 (1987).

[15] I. V. Hertel and W. Stoll, Adv. At. Mol. Phys. **13**, 113 (1978).

[16] U. Fano, J. Opt. Soc. Am. **39**, 859 (1949).

[17] C. H. Greene and R. N. Zare, J. Chem. Phys. **78**, 6741 (1983).

[18] A. R. Edmonds, *Angular Momentum In Quantum Mechanics* (Princeton University, Princeton, 1974).

[19] S. N. Dixit and V. McKoy, J. Chem. Phys. **82**, 3546 (1985).

[20] E. Hecht and A. Zajac, *Optics* (Addison–Wesley, Reading, MA, 1974).

[21] D. M. Brink and G. R. Satchler, *Angular Momentum* (Clarendon, Oxford, 1968).

[22] J. Mathews, *Tensor Spherical Harmonics* (Graphic Arts, Cal. Inst. of Technology, 1981).